The Combustion Driven Shock Tube
Ae 104c Final Report

Brock Bobbitt, Sermet Şahaner, Bryan Schmidt

June 9, 2012

1 Abstract

A combustion driven shock tube was designed, constructed, and first tested using helium in the driver section and air in the driven section and then with hydrogen, oxygen, and helium in the driver section and air in the driven section. The shock tube is also modeled using a software package called Cantera. Shock speed measurements from helium shots agree with at most 20% disagreement with ideal theory, and the disagreements are explained by well-documented non-ideal effects. Pressure measurements are consistently lower than predicted. Because of safety concerns, the pressure in the driver section for combustion shots had to be lowered from the originally intended value of 20 bar to 1 bar, resulting in a much lower reaction rate. As a result, a well-functioning combustion-driven driver section was not obtained. Modifying the system by either alleviating safety concerns and operating at full scale or altering the driver mixture to make one more favorable for combustion would make the shock tube fully functional as intended.

Contents

2 Introduction

2.1 Basics of shock tube operation

Shock tubes are an important experimental tool for investigating unsteady gas dynamics, chemical kinetics, and other processes at high temperatures and pressures. A shock tube is formed by a vessel that contains a gas at high pressure and a gas at low pressure separated by a diaphragm. The high-pressure section is called the driver section and the low-pressure section is called the driven section. Figure 1 shows a diagram of a simple shock tube. When the diaphragm is removed suddenly, a compression wave propagates into the driven section, and this compression rapidly steepens into a planar normal shock wave. At the same time, an isentropic expansion wave propagates into the driver section. Expansion waves do not cause abrupt changes in pressure, so they are often referred to as "fans." In between the shock wave and expansion fan is a dividing line between the gas originally in the driven section and the gas originally in the driver section called a contact surface [5]. When the shock reaches the end of the tube, it reflects off the end wall and propagates back towards the contact surface, where it reflects again. Figure 2 is an x-t diagram of the ideal shock tube problem.

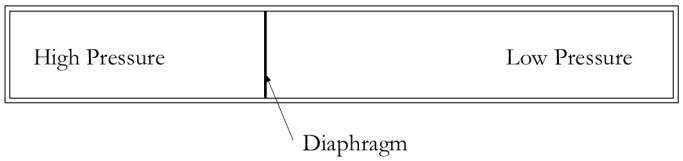

Figure 1: Diagram of a simple shock tube

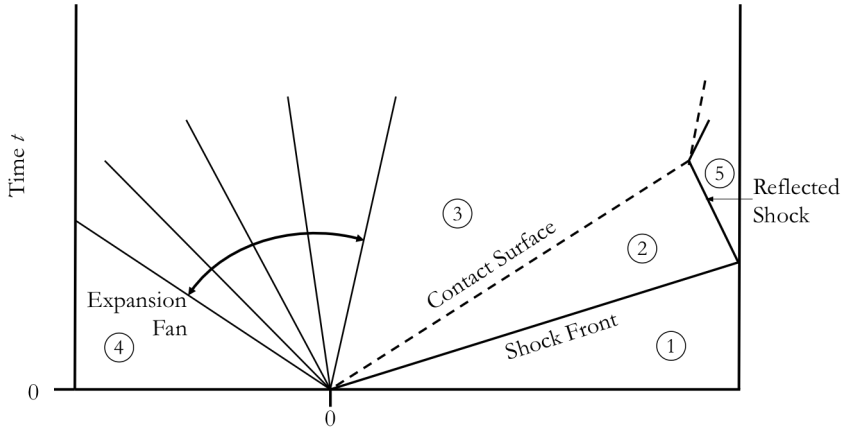

Figure 2: x-t diagram

The regions labeled 1-5 represent five very different physical states. Region 1 is the state in the driven section before the shock passes through it, region 2 is the driven gas after the normal shock has passed through it, region 4 is the initial state in the driver section, region 3 is the gas in the driver section after it has been expanded, and finally region 5 is the driver gas after the reflected shock has passed through it. Region 5 exhibits the highest pressure and temperature of these five states. It would be useful to find a relation that could predict the performance of the shock tube, namely the Mach number of the shock produced, based on the initial states 1 and 4.

The pressure ratio $\frac{p_4}{p_1}$ can be expanded as follows:

$$\frac{p_4}{p_1} = \frac{p_4}{p_3}\frac{p_3}{p_2}\frac{p_2}{p_1} \tag{1}$$

For perfect gases, the right hand side of equation 1 can be related to the properties of the gases and their velocities. $\frac{p_4}{p_3}$ follows from an expansion wave propagating into a stationary gas.

$$\frac{p_4}{p_3} = \left(1 - \frac{\gamma_4 - 1}{2}\frac{u_3}{a_4}\right)^{-\frac{2\gamma_4}{\gamma_4 - 1}} \tag{2}$$

Here, a_k represents the speed of sound in region k, $\sqrt{\gamma_k R_k T_k}$. Velocity and pressure are matched across the contact surface, so $\frac{p_3}{p_2} = 1$. $\frac{p_2}{p_1}$ can be expressed in terms of the shock Mach number using the normal shock relations for a perfect gas.

$$\frac{p_2}{p_1} = 1 + \frac{2\gamma_1}{\gamma_1 + 1}(M_s^2 - 1) \tag{3}$$

The Mach number of the shock is defined as the ratio of the speed of the shock to the speed of sound ahead of the shock, $\frac{u_s}{a_1}$. With the knowledge that the velocity is matched across the contact surface, i.e. $u_3 = u_2$, the only missing piece of information is to relate u_2 to the shock Mach number M_s. This also follows from the normal shock relations for a shock propagating into a stationary perfect gas.

$$\frac{u_2}{a_1} = \frac{2}{\gamma_1 + 1}\frac{M_s^2 - 1}{M_s} \tag{4}$$

Combining equations 1-4 yields the shock tube equation:

$$\frac{p_4}{p_1} = \frac{1 + \frac{2\gamma_1}{\gamma_1+1}(M_s^2 - 1)}{\left(1 - \frac{\gamma_4 - 1}{\gamma_1 + 1}\frac{a_1}{a_4}\frac{M_s^2 - 1}{M_s}\right)^{\frac{2\gamma_4}{\gamma_4 - 1}}} \tag{5}$$

From this equation, it can be observed that the strength of the shock produced in a shock tube is a function of the initial pressure ratio between the driver and driven gases $\frac{p_4}{p_1}$, the ratios of specific heats of the driver and driven gases γ_k, ratio of the specific gas constants of the driver and driven gases R_k, and the ratio of the temperatures between the driver and driven sections T_k [8].

Behind the reflected shock, the velocity is zero which allows the pressure ratio across the reflected shock $\frac{p_5}{p_2}$ to be expressed in terms of the pressure ratio across the incident shock $\frac{p_2}{p_1}$ [4].

$$\frac{p_5}{p_2} = \frac{(3\gamma_1 - 1)\frac{p_2}{p_1} - (\gamma_1 - 1)}{(\gamma_1 - 1)\frac{p_2}{p_1} + (\gamma_1 + 1)} \tag{6}$$

2.2 Combustion driven shock tube

Further inspection of equation 5 reveals that as the pressure ratio $\frac{p_4}{p_1}$ approaches infinity, the shock Mach number reaches a maximum value for fixed gas properties, namely

$$\frac{M_s^2 - 1}{M_s} \rightarrow \frac{a_4}{a_1}\frac{\gamma_1 + 1}{\gamma_4 - 1} \tag{7}$$

For many applications, high shock Mach numbers are very desirable because they create the largest values for p_5 and T_5 after the reflected shock, as can be observed from equations 3 and 6. Varying the gases in the driver and driven sections is one way to produce higher Mach numbers because $\frac{a_4}{a_1}$ varies approximately as $\sqrt{\frac{W_1}{W_4}}$ where W_k represents the molecular weight of gas k. Even with this added influence, though, the pressure ratios required to produce strong shocks are rather high.

An excellent method to encourage strong shocks by both increasing the sound speed ratio and the pressure ratio between the driver and driven sections is to use a combustion driver. Combustion in the driver section simultaneously raises the driver pressure p_4 and temperature T_4, which in turn increases a_4.

Typicall combustion drivers combust a mixture of hydrogen and oxygen diluted with helium because it allows for efficient combustion while maintaining a low value for γ_4 because of the helium diluant [5].

In this experiment a combustion driven shock tube is designed, constructed, and tested using a driver section originally built by Bélanger for his Ph.D. thesis in 1993. The goal is to create a shock tube capable of generating strong shocks ($M_s \gtrsim 7$) in air driven by the combustion of stoicheometric hydrogen and oxygen with a helium diluant. An important requisite for this goal is the capability to accurately measure the initial conditions in both sections of the shock tube and the speed of the shocks produced. An additional goal is to explore the ability to model the shock tube and accurately predict shock properties based on initial conditions using a software tool called Cantera that is used for modeling chemical kinetics, thermodynamics, and transport processes.

3 Layman's Introduction

Shock tubes are used in order to produce shock waves and high speed flows. The test times are very short, on the order of a millisecond, but this is often long enough to gather interesting information. Shock waves and high speed flows are produced by exposing a higher pressure gas to a lower pressure gas. A shock tube does this by using two pipes separated at their ends by a very thin piece of material called a diaphram. One pipe, the driver section, is brought to a higher pressure than the second, the driven section, then the diaphram is burst using one of various mechanisms. By rupturing the diaphram quickly, the higher pressure gas is is exposed to the lower causing a shock wave and high speed flow to travel down the driven section.

The interest of this experiment is to generate and study as high of shock speeds as possible. The speed of the traveling shock wave is determined by the pressure ratios between the driver and driven gases and the speed of sound of the driver gas, a seen in equation 5. One clever way to increase the pressure ratio and the driver gas speed of sound is to use combustible gases in the driver section and combust them slightly before rupturing the diaphram. In this way, the exothermic chemical reation will produce heat, increasing the temperature of the driver gas. This both increases the driver gas pressure and speed of sound. Therefore both results are effective in increasing the shock speed. In order to study and employ very high speed shock waves, this purpose of this study is to build and test a combusion driven shock tube.

4 Experimental Setup and Procedure

4.1 Driver Section

The only primary component in the setup that was not specifically designed for this experiment is the driver section. The driver is constructed from a 1.5 m long stainless steel tube. The tube has an inner diameter of 5 cm with a wall thickness of 1.9 cm. The product of the combustion reaction between hydrogen and oxygen in the driver is water vapor, which necessitates stainless steel to avoid corrosion. Figure 3 shows a schematic of the driver section (not to scale).

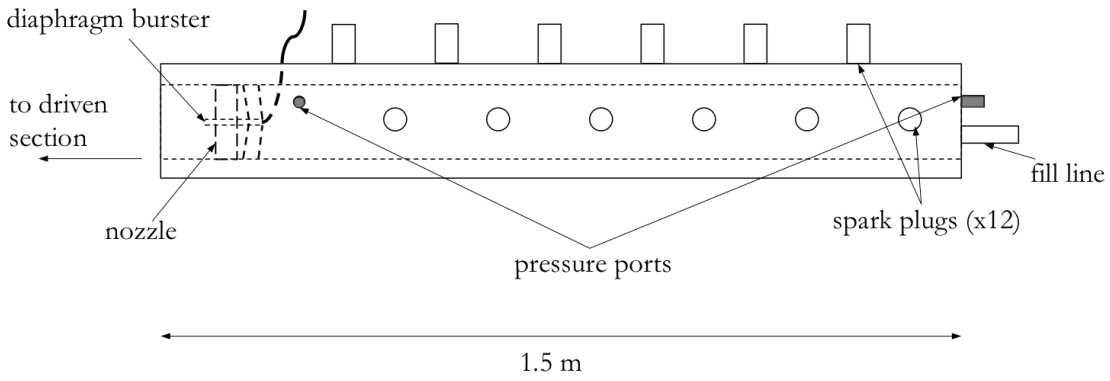

Figure 3: Driver section schematic

To initiate combustion, the tube is lined with two rows of six automotive-type spark plugs evenly distributed along the length of the tube. The rows are oriented at 90 degrees relative to each other. Distribution of the ignition sources minimizes the risk of detonation in the tube. Each spark plug is connected its own electrical circuit and 20 kV capacitor. When the system is triggered, the trigger is sent simultaneously to all twelve circuits. The system was originally designed to test at filling pressures above 2 MPa, so the gaps between the electrodes of the spark plugs were reduced from 2 mm to 1 mm [2]. Figure 4 shows a photograph of the driver section in which the spark plugs are clearly visible. All of the electronics for the spark plugs as well as for the diaphragm bursting system are housed in aluminum boxes which can be seen on the table next to the driver in figure 4.

Figure 4: Driver section mounted to rails

The driver is designed to withstand internal pressures up to 35 MPa, taking into account stress concentrations due to holes from spark plugs and pressure ports. Bélanger successfully operated the tube up to pressures of 20 MPa after combustion, and advises a maximum pressure after combustion of 25 MPa for testing [2].

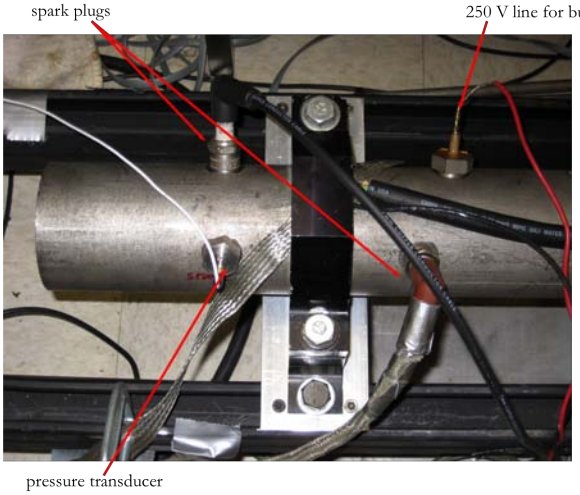

Figure 5: End of driver section closest to diaphragm

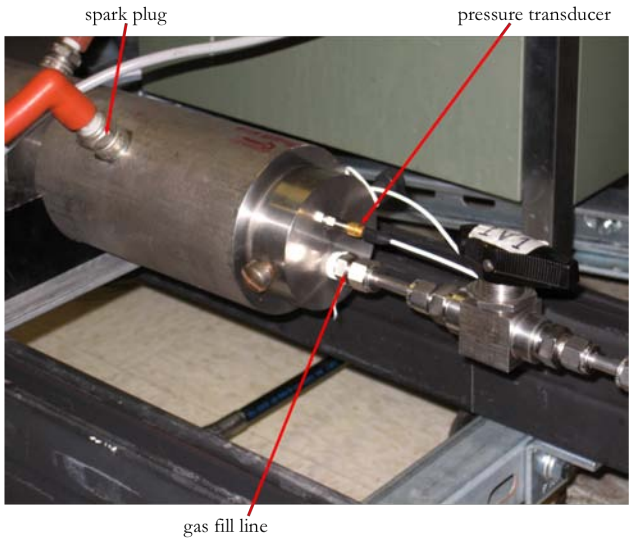

Figure 6: Endcap of driver section

There are two ports in the driver section to measure the pressure. One is located near the diaphragm, 11 cm away from the closest spark plug to the driven section, and the other is situated in the endcap. The fill line also enters through the endcap. Figures 5 and 6 show the locations of the pressure transducers in the driver. The purpose of these transducers is to measure the pressure rise due to combustion before the diaphragm is broken. Both transducers were originally intended to be PCB 113A22's, which can measure pressures up to 34 MPa. This was later changed, for reasons that will be discussed.

The fill line enters the driver section at about a 30 degree angle relative to the centerline of the driver to encourage mixing. This was necessary for Bélanger who attempted to mix the hydrogen, oxygen, and helium in the driver section, but it is not necessary for this experiment in which an external mixing tank is used to mix the driver gases before the driver is filled.

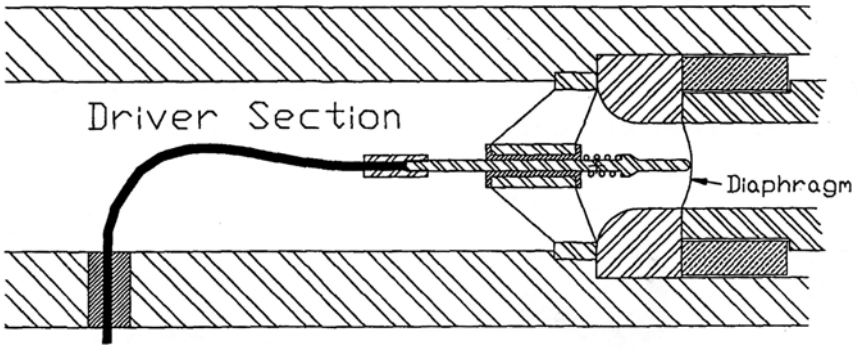

Figure 7: Schematic view of diaphragm bursting system inside the driver [2]

A somewhat unconventional method is used to burst the diaphragm. The original purpose of the driver required that the diaphragm bursting system be able to burst the diaphragm with an accuracy of at least 0.2 ms. A combustion process is not repeatable to that accuracy, so another method was developed. A 5 mf capacitor at 250 V is discharged into the diaphragm using a probe. When the driven section is slid into place to mate with the driver section, the diaphragm is pressed against the probe, which is spring-loaded to ensure the diaphragm is not punctured by the pressure of the probe alone. This arrangement can be seen in

figure 7, taken from Bélanger's thesis. The total resistance in the line between the capacitor and the probe is 0.05 Ω. The tube itself is grounded to the structural members of the room, making it the ground of the system [2]. The electrical discharge from the probe melts the diaphragm in its center, weakening it, and the pressure difference between the driver and driven sections forces the diaphragm to open fully.

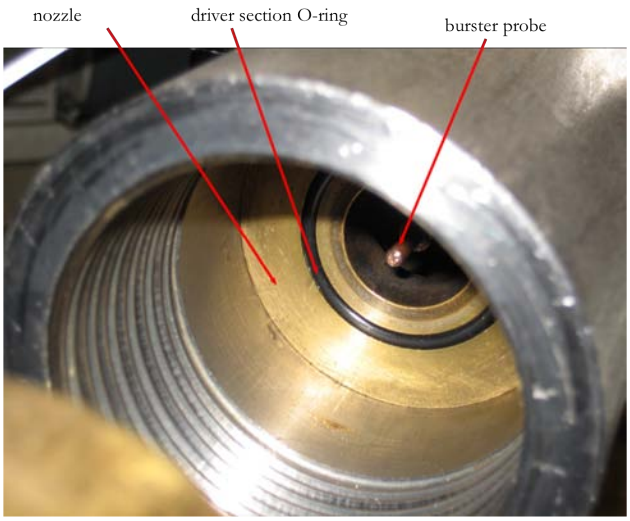

Figure 8: Location of diaphragm in the driver section, note that the probe of the diaphragm burster is visible in the center of the brass nozzle. Also note the threads on the inside of the driver section that mate with the driven section.

When the diaphragm is inserted, it is pressed into an O-ring on the downstream side of a brass nozzle which is situated between the driver and driven sections. The nozzle reduces the diameter of the tube from 5 cm in the driver to 2.54 cm in the driven section. The O-ring helps create a seal between the two sections of the shock tube. Figure 8 shows a photograph of the O-ring and nozzle. The probe of the diaphragm is also visible in the figure.

Aluminum diaphragms were initially used, but they were found to not break properly with the burster system. Stainless steel diaphragms are used instead because stainless steel has a lower electrical conductivity than aluminum, so they are much easier to melt with the probe, creating a larger initial hole in the diaphragm. Additionally, Bélanger suggests that cracks propagate better in the steel diaphragms than in the aluminum ones. The primary disadvantage of the steel diaphragms is that fragments from burst diaphragms detach and are sent down the tube, which is not ideal and requires regular cleaning of the driven section between shots [2]. Figure 9 shows the result of an unsuccessful attempt to burst an aluminum diaphragm, and figure 10 shows a burst steel diaphragm.

Figure 9: An unbroken aluminum diaphragm. The probe burned a very small hole in the center of the diaphragm, but the pressure difference between sections was unable to force the diaphragm the remainder of the way open.

Figure 10: A broken steel diaphragm. Notice that the majority of the center of the diaphragm has been broken and the fragments have been sent down the tube.

Bélanger was able to relate the thicknesses of the steel diaphragms to the pressure difference required to burst them. This information is presented in table 1. These pressures after combustion correspond to fill pressures ranging from 200 kPa to 2 MPa.

Diaphragm Thickness (mil)	Max Pressure for Tests (MPa)	Min Pressure for Tests (MPa)
1	1.0	0.3
2	3.5	2.0
3	5.5	3.5
4	7.0	5.5
5	9.0	6.5
8	14.5	9.0
12	22.0	14.0

Table 1: Diaphragm thicknesses with corresponding maximum and minimum pressures (after combustion) for tests [2]

4.2 Driven Section

The driven section of the shock tube was designed specifically for this experiment. Like the driver, it is also constructed of 304 stainless steel. The driven section is 1.37 m long with an inner diameter of 2.54 cm. The thickness of the wall is 1.27 cm. Figure 11 shows a schematic of the driven section, and a dimensioned drawing of the driven section can be found in appendix A. The dimensions of the driven section are chosen to minimize the effect of the boundary layer behind the shock decelerating the shock wave. In his work on finding the limitation on test time for laminar and turbulent boundary layers in shock tubes, Mirels suggests a length/diameter ratio of approximately 50 for a driven section tube such as this one [7].

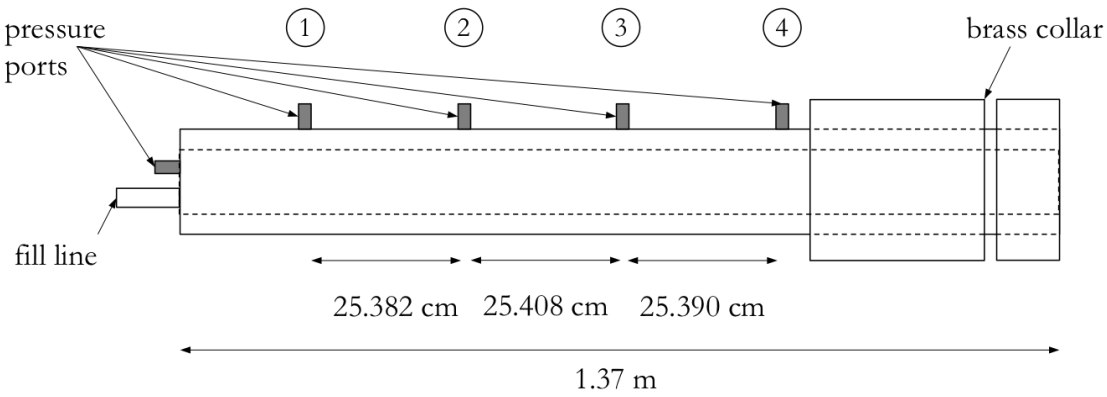

Figure 11: Driven section schematic

The driven section attaches to the driver section by means of an internally threaded brass collar ring that screws onto the end of the driven section and presses the diaphragm against the nozzle and an externally threaded brass collar that mates to the internally threaded driver section. The internally threaded collar also has an O-ring to seal against the diaphragm on the opposite side of the nozzle. Figure 12 shows the two brass collars and the O-ring. The collars and mating method were used by Bélanger.

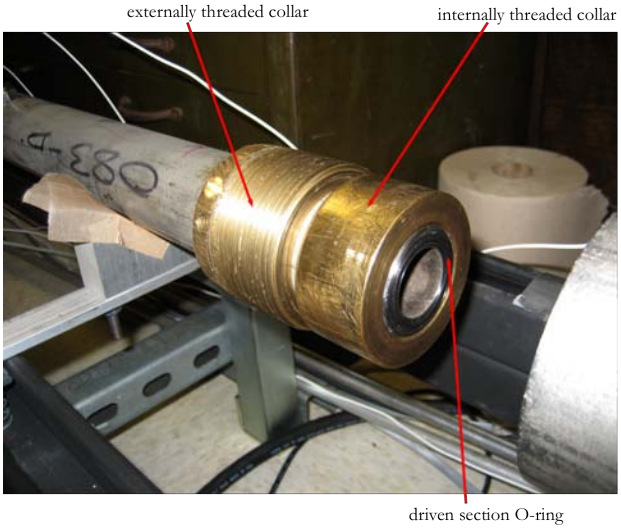

Figure 12: Brass collars on the end of the driven section. Note that the externally threaded collar is situated behind the internally threaded one and is free to slide along the tube until it is mated to the driver.

Five pressure transducers are incorporated into the driven section, one in the endcap and the other four equally spaced along the length of the tube. Their primary purpose is to measure the speed of the shock as it propagates through the driven section as well as to measure the pressure jump caused by the shock. The measured distances between transducers along the length of the driven section are given in figure 11. All five are PCB 113A21 transducers, capable of measuring pressures of up to 1.38 MPa. These transducers have a response time of 1 μs, which is required to precisely find the time of arrival of the shock front. The data from all seven pressure transducers is sent to a National Instruments PCI-6133 data acquisition card using a PCB 481 signal conditioner.

To approximate the limiting pressure of the driven section considering the stress concentrations created

by the holes created for the pressure transducers, a simple finite element analysis is performed on a hole to find the stress concentration factor. The driven section must be analyzed as a thick-walled tube, so the Lamé solution must be implemented. Radial stress will be negligible compared to the hoop stress, but the hoop stress is comparable to the stress in the axial direction. From the Lamé solution for zero external pressure, inner radius a, and outer radius b, the maximum stress in the thickness is:

$$\sigma_{\theta\theta} = \frac{a^2 p}{b^2 - a^2}\left(1 + \frac{b}{a}^2\right) = \frac{a^2 + b^2}{b^2 - a^2}p \tag{8}$$

For $a = 1.27$ cm and $b = 2.54$ cm, the expression simplifies to $\sigma_{\theta\theta} = \frac{5}{3}p$. The axial stress in turn is related to the internal pressure as follows.

$$\sigma_{zz} = \frac{a^2}{b^2 - a^2}p \tag{9}$$

Plugging in numbers, this becomes $\sigma_{zz} = \frac{1}{3}p$. Therefore the hoop stress is five times larger than the axial stress. VisualFEA was used to perform a simulation of loading a small plane section with a hole to find the stress concentration at the hole. This plane analysis does not take the curvature of the pipe into account, but the member being analyzed is small so the approximation is still valid. Symmetry is exploited to reduce computation, as only a quarter of the hole is analyzed. The other parts of the member are replaced by zero-displacement conditions perpendicular to the cuts. The remaining two sides of the rectangular member are loaded with an evenly distributed load with one side being five times larger than the other to simulate the loading condition when the pipe is under pressure.

The results are shown in figure 13. Relevant material properties are an elastic modulus of 193 GPa for the pipe which is stainless steel and a modulus of 197 GPa for the pressure transducer mounting adapter which is a PCB 061A01 made from 17-4 PH stainless steel. Analysis reveals a stress concentration factor of about 1.5. Here the stress concentration factor is defined with respect to the internal pressure instead of a characteristic stress, i.e. $K = \frac{\sigma_{vM}}{p}$ where σ_{vM} is the von Mises stress, important in determining yielding behavior.

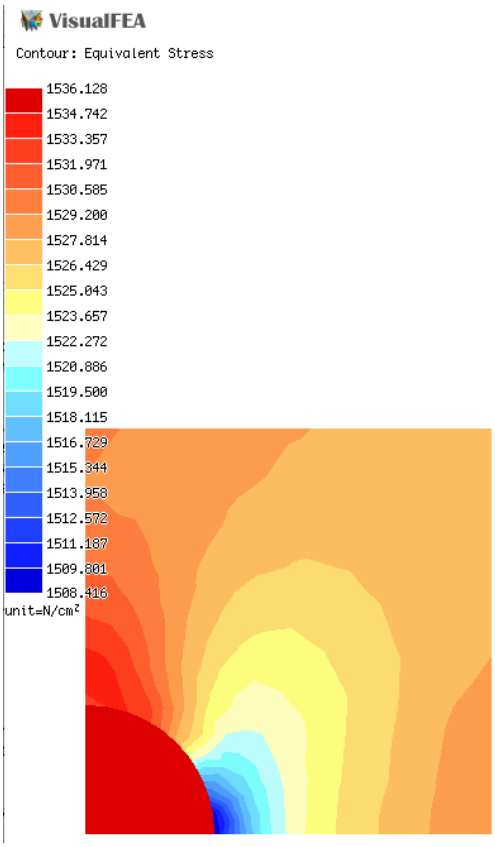

Figure 13: Contour plot of von Mises stress for stainless steel with a circular 17-4 PH stainless steel plug with an internal pressure of 1000 N/cm^2

Since the yield strength of 304 stainless steel is approximately 275 MPa and much smaller than the yield strength of 17-4 PH stainless steel, the maximum pressure sustainable by the driven section is approximately 180 MPa. Cantera predicts a maxium pressure behind the reflected shock (p_5) of about 150 MPa for the largest pressure rise expected in the tube, which would occur with an initial fill pressure p_4 of 2 MPa and a value for p_1 of 100 kPa. p_1 will typically be much smaller than this to encourage higher Mach number shocks. Multiple approximations were made in this stress analysis, but these results suggest that the driven section is sufficiently robust to function without failure in all environments it will experience because the most conservative estimates were used during calculations.

The endcap of the driven section houses both a pressure transducer and a gas line. This line is used both to vacuum the driven section as well as to fill the section with air to the desired value of p_1. The endcap is shown in figure 14.

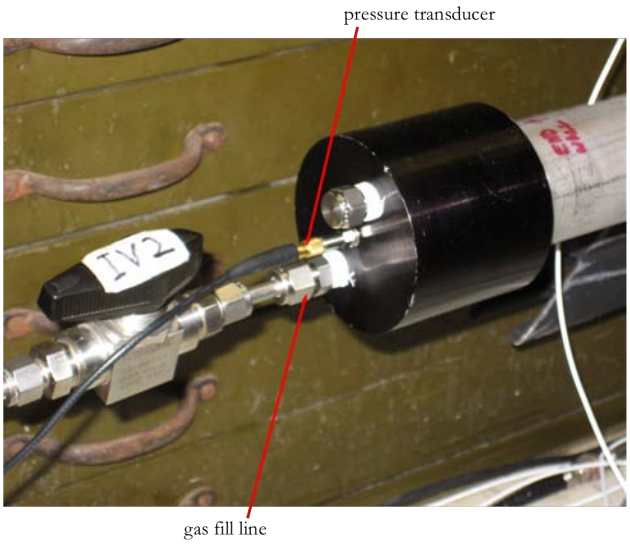

Figure 14: Driven section endcap. The unlabeled extrusion from the endcap is a plug for an improperly drilled hole.

Figure 15 shows the driven section in its fully assembled configuration with pressure transducers installed.

Figure 15: Fully assembled driven section. The large black cable visible is a grounding cable for the driven section to decrease interference from the diaphragm bursting system to the pressure transducers.

4.3 Gas Lines

Ensuring that the driver gases are well-mixed before combustion is crucial to achieving the desired performance of the shock tube. The method used by Bélanger of mixing the gases in the driver section is not sufficient to fully mix the gases, as stated by Bélanger himself [2]. The mixing tank for the GALCIT 6-inch shock tube is therefore used to mix the hydrogen, oxygen, and helium for the driver section before filling the driver. Fill lines for the mixing tank as well as the infrastructure necessary to contain gas bottles already existed in the facility, so the only necessary step was to develop a plumbing network that would allow the combustion driven shock tube to tap into the existing gas lines. Figure 16 shows the mixing tank, existing gas line panel, and added lines and valves for the combustion driven shock tube.

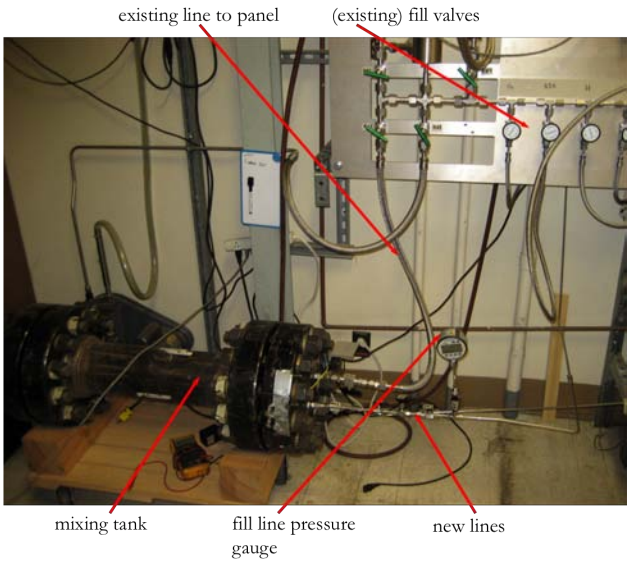

Figure 16: Tank, fill line panel, and new gas lines and valves

Other valves and gas lines were added to facilitate evacuating, filling, and venting the shock tube. A full schematic of the plumbing is shown in figure 17. Table 2 lists each new valve along with its make, model, and maximum pressure rating.

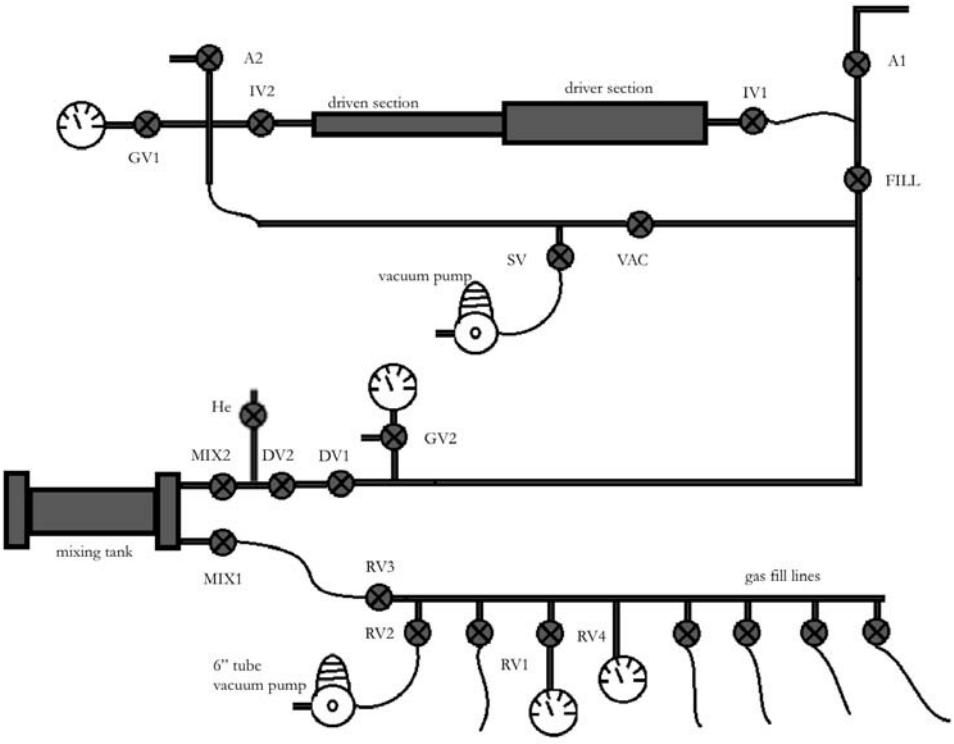

Figure 17: Plumbing diagrams. Valves are named according to how they are labeled in the laboratory.

Valve(s)	Make and Model	Valve Type	Maximum Pressure Rating (MPa)
IV2	Whitey SS-83-KS4	Ball	41.4
A2	Swagelok SS-4PAT	Slotted Ball	unknown
SV, VAC, FILL, DV1, He	Swagelok SS-42S4	Ball	17.2
IV1, MIX1	Swagelok SS-83KS4	Ball	41.4
A1, MIX2	Swagelok SS-43S4	Ball	20.7
DV2	Swagelok SS-1RS4	Needle	20.7
RV1, RV2, RV3, RV4	Swagelok SS-8B6-V47	Needle	6.9
gas fill line valves	Swagelok SS-4B6-V51	Needle	6.9
GV1, GV2	Swagelok SS-43XS4	3-way Ball	17.2

Table 2: Valve makes, models, types, and maximum pressure ratings for all valves in the apparatus

4.4 Infrastructure

The shock tube was originally intended to be mounted to an optical table, but the necessity of being in close proximity to the mixing tank for the GALCIT 6-inch shock tube forced an alternative design. The shock tube is instead mounted to a rack built from Unistrut rails. Two supports like the one shown in figure 18 were built by Bélanger to support the driver section. One of these has a matching part that fits over the top of the driver to secure it into place. Aluminum plates were made to mount these supports onto the rails. A drawing for these plates can be found in appendix A.

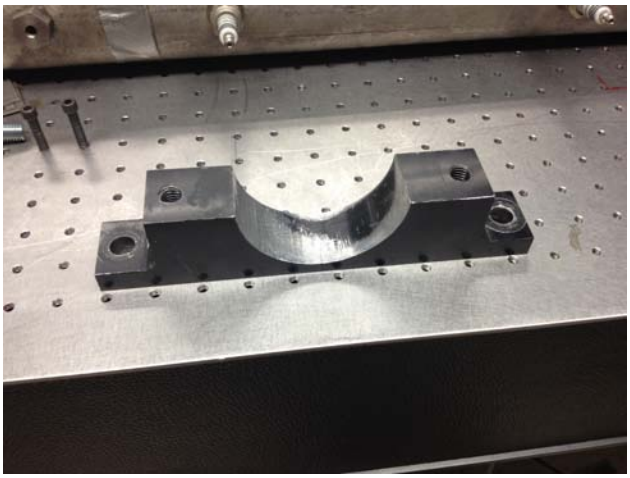

Figure 18: Driver support

The driven section is supported by a pair of aluminum V-blocks which are secured to the Unistrut rails by smaller aluminum plates. Drawings for these parts can also be found in appendix A. The V-blocks are carefully designed so that the driver section is concentric with the driven section so that they mate together neatly. The surfaces in contact between the V-blocks and the tube are coated in teflon tape to minimize wear resulting from friction when the driven section is slid out from the driver section on the blocks. Figure 19 shows the complete assembly of the shock tube on the rails. The electrical components are mounted to a large aluminum plate to simplify grounding.

Figure 19: Full assembly of shock tube and electrical components

4.5 Experimental Procedure

Basic operation of the system is first conducted with pure helium at high pressure in the driver section and air at low pressure in the driven section. In this configuration, the combustion driven shock tube operates like a standard shock tube except for the diaphragm bursting device. Helium shots allow components of the system such as the plumbing, diaphragm bursting device, vacuum pumps, and data acquisition system to be tested without the complication of combustion in the driver section. The data from the helium shots can be analyzed just like data from any conventional shock tube and can be compared with the predictions made by Cantera. Certain properties such as the pressure difference required to burst a diaphragm of a given thickness can also be investigated.

After the system is fully tested using helium shots, shots with combustion in the driver are performed. Data from Bélanger suggests that the best mixture of the driver gases is 79% helium, 14% hydrogen, and 7% oxygen by volume. This produces the largest pressure rise without causing detonation waves in the driver section [2].

Testing proceeds in the following manner. First, the mixture is prepared in the mixing tank. For helium shots, this is as simple as filling the mixing tank to the desired pressure with helium alone. For combustion shots, the mixing tank is filled using Dalton's law of partial pressures. The tank is filled with helium first to ensure that when the combustible mixture is formed it will already be diluted, decreasing the risk of premature combustion. Once the desired partial pressure of helium is reached, the tank is closed and the fill lines for the tank are evacuated. The tank is then filled to the proper pressure with oxygen and finally hydrogen, evacuating the fill lines in between filling with each individual gas. Once the mixing tank is full, the gases are mixed for several minutes using the mixing fan built into the tank.

After preparing the mixture, diaphragm is placed between the two sections of the shock tube, the sections are secured together, and the entire shock tube and all fill lines between the tube and the mixing tank are evacuated using a vacuum pump. Once a suitable vacuum is reached, the pressure in the driven section p_1 is set using a small valve open to the atmosphere to raise the pressure up to the desired value. The fill pressure p_4 is then set in the driver section by filling from the mixing tank. Once both pressures have been reached, the isolation valves (labeled IV1 and IV2 in figure 17) on either side of the shock tube are closed and the

capacitors for the spark plugs and diaphragm bursting system begin to charge.

At this time, the data acquisition system is armed by running a MATLAB script that can be found in appendix B. Once the DAS is armed and the capacitors are charged, the trigger signal is sent to fire the shock tube. A signal is immediately sent to the spark plug circuits to begin combustion (in the case of a combustion shot). 40 ms is allowed for combustion to take place, a value suggested by Bélanger [2]. After 40 ms, two signals are sent simultaneously, one to the diaphragm burster circuit to burst the diaphragm and another to the DAS to begin recording data. Data files are automatically saved.

After a shot, the electrical components are switched off to avoid an unexpected discharge. After this, the shock tube is vented to the atmosphere and both the tube and the fill lines are flushed with helium to ensure that any combustible gases are pushed safely out of the apparatus. The diaphragm is then removed and any diaphragm fragments are cleaned out of the driven section with compressed air. The full checklist used during experiments can be found in appendix C.

The speed and strength of the incident shock wave can be determined from plotting pressure vs. time for each of the pressure transducers along the length of the driven section. The speed of the wave is determined by finding the difference in time of arrival between two adjacent transducers and dividing the distance between those transducers by that time difference. The three resulting speeds from the three gaps between transducers are then averaged to compute a final value. The pressure jump $p_2 - p_1$ can be determined directly from the pressure traces.

4.6 Numerical Predictions with Cantera

In order to attempt to predict performance of the combustion driven shock tube, a software package called Cantera is used. Cantera can be used as a toolbox in MATLAB, allowing the user to write routines in MATLAB that can call Cantera. Cantera is used to model chemical processes, thermodynamics, and transport processes.

The first step in the MATLAB routine for the combustion driven shock tube is to calculate the temperature, pressure, and constituents of the mixture in the driver section after combustion. It does this based on the initial constituents, fill pressure, and temperature by calling Cantera to calculate the equilibrium pressure and temperature for a completed chemical reaction between the initial constituents while holding internal energy and volume constant. Holding internal energy constant is considered to be a reasonable approximation because the combustion process takes place over a very short time scale so only a small amount of heat is lost to the walls of the tube. Cantera also calculates the concentrations of individual species in the driver section after combustion.

After these calculations, the routine uses a shooting method to solve the shock tube equation (equation 5) for Mach number based on pressure after combustion in the driver p_4', the pressure in the driven section p_1, the temperatures in each section, and the gases in each section. Once the shock Mach number is obtained, calculating the conditions in states 2 and 5 from the perfect gas equations is straightforward. The final step taken in the routine is to allow Cantera to predict dissociation of gas species behind the incident and reflected shocks based on the temperature and pressure in those regions.

The full script used can be found in appendix B.

5 Safety Considerations and Resulting Modifications

A short time after the construction of the infrastructure, plumbing, and shock tube was completed, a laboratory accident occurred during a separate experiment with a similar procedure to the one used in this experiment. A premixed stoicheometric mixture of ethylene and oxygen at 345 kPa was being pumped from an external mixing tank to the experimental vessel. When a valve was closed, an unexpected detonation occured in the fill line which caused failure of plumbing components and significant damage to the apparatus. The valve was turned remotely from a protected room so no individuals were harmed. The exact mechanism for this detonation is uncertain, but it has been hypothesized that unsteady gas dynamics resulting from the rapid closing of a ball valve could have influenced a large enough temperature rise to cause combustion

which led to a detonation of the combustible mixture. Figure 20 shows the result of the detonation in a section of tubing close to the valve that was closed.

Figure 20: Result of a detonation in the fill line in a similar experiment

Recall that the combustion driven shock tube is designed to operate at fill pressures up to approximately 2000 kPa, which at 79% helium corresponds to a partial pressure of 420 kPa of combustible mixture. Additionally, in the plumbing scheme all valves are turned manually, leaving the operators dangerously close to the combustible mixture if a detonation were to occur. Therefore the fill pressure must be reduced to a value such that if a detonation were to occur in the fill lines there would be no failure of components. The lowest rated pressure of any of the plumbing components including the tubing is the 17.2 MPa of the Swagelok SS-42S4 ball valves. It was determined from Cantera that a stoicheometric mixture of hydrogen and oxygen at 100 kPa were to combust and then have a deflagration to detonation transition (DDT), the final pressure would be approximately 17 MPa. This includes an estimation of a factor of two pressure rise from Chapman-Jouguet theory and another factor of five for DDT.

As a result, a maximum fill pressure of 100 kPa was set for safety reasons, although the mixture would remain 79% helium, 14% hydrogen, and 7% oxygen. Cantera predicts a final pressure after combustion of 750 kPa for this mixture. This resulted in modifications to the system. First, it was found that combustion did not occur in the driver at 100 kPa fill pressure, even though the mixture is well within the flammable region proposed by Holmstedt for hydrogen, oxygen, and helium mixtures [6]. It was hypothesized that the small gaps between the electrodes in the spark plugs were close enough to quench the reaction due to heat transfer to the electrodes themselves since pressure has a strong effect on quenching distance for a given mixture. The electrode gaps were originally set to 1 mm to achieve combustion in high-pressure mixtures. The gaps were readjusted to 1.5 mm, which allows combustion to occur.

Secondly, since the Mach number of the shock depends on the ratio between driver and driven pressures and not the values of pressure themselves, as evidenced by equation 5, the pressures used in the driven section are reduced significantly from several kPa to a few hundred Pa to achieve the high Mach numbers desired. Because of the smaller pressure difference between p_4' and p_1, only the 1 mil steel diaphragms can be used. These very thin diaphragms very easily buckle under the spring load from the diaphragm burster probe, ruining the pressure seal for the driver section. The spring in the probe apparatus was replaced with a less stiff one, but even so properly securing a 1 mil steel diaphragm into place remains a delicate and time-consuming procedure.

Because of a much smaller pressure in the driver section after combustion than was originally intended, the PCB 113A24 closest to the diaphragm in the driver section is replaced by a PCB 113A24, which is sensitive up to 6.8 MPa instead of 34 MPa.

6 Measurement Accuracy

This study seeks to measure the initial shock wave speed and the pressure jump across the shock. In order to calculate these values, two types of measurments are required, pressure and distance. Four pressure measurements will be aquired at fixed locations along driven section. The distances, d_n between these transducers was measured using a verneir caliper. Regarding the shock speed, through two pressure measurments, the time, t_n, between arival of the shock at each location is calculated. Therefore the shock speed is calculation through equation 10 and the pressure jump through equation 11. The subscript m is to specify which pair of transducers is used to make the calculation, while subscript n refers to each pressure transducer.

$$V_m = \frac{d_m}{t_m} \tag{10}$$

$$p_n = p_{a,n} - p_{b,n} \tag{11}$$

Figure 21 shows the data output from all of the pressure transducers in the driven section. The incident shock is clearly visible as four sharp jumps in the pressure traces. The large amplitude oscillation near $t = 0$ is the result of electrical interference from the large discharge from the bursting of the diaphragm.

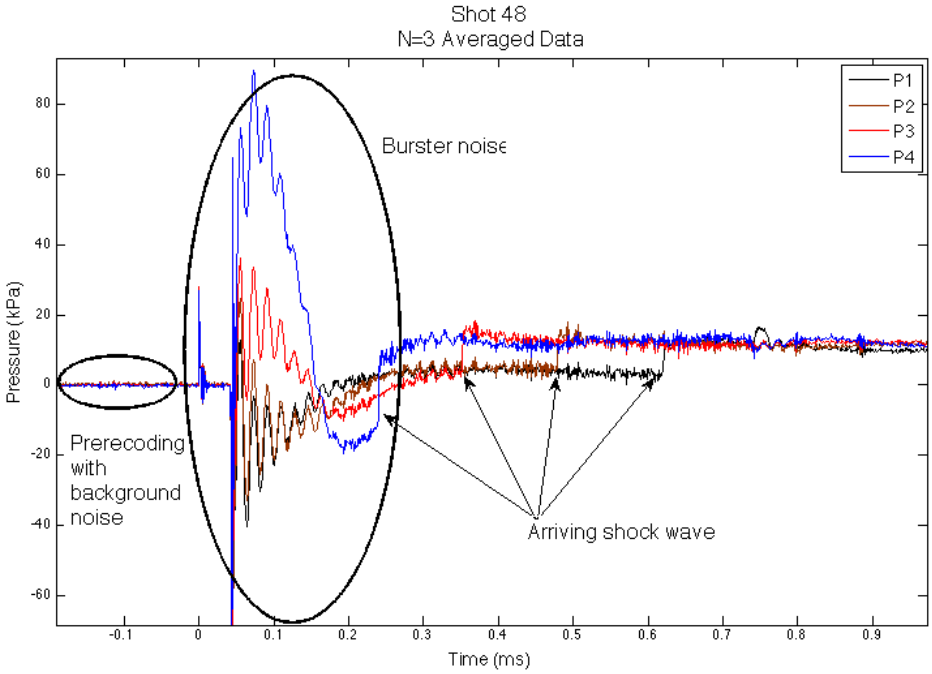

Figure 21: Typical data output from a helium shot

6.1 Shock Velocity

The measurement uncertainty V_m, denoted, δV_m, depends on the uncertainty in the distance between the transducers and the time of shock speed arrival and is determined as follows.

$$\delta V_m = \delta \frac{d_m}{t_m} \tag{12}$$

$$\frac{\delta V_m}{V_m} = \sqrt{\left(\frac{\delta d_m}{d_m}\right)^2 + \left(\frac{\delta t_m}{t_m}\right)^2} \tag{13}$$

Therefore, to determine the uncertainty in velocity, the uncertainty in the distance and time is required. To determine the distance between the pressure probes, two measurements were used: the distance between the outside of two probes, and the diameter of the probes. Therefore, δd_m is twice of both uncertainties. Through repitition of the measurement between the outside of the pressure probes, an approximate measurement uncertainty was found to be $1.27 * 10^{-4}$ m. This is the average difference between multiple measurements. Therefore $\delta d_m = 2.54 * 10^{-4}$ m.

Regarding, δt_m, two sources contribute to this measurement uncertainty. First is the rise time of the pressure transducer. All transducers on the driven section are PCB model 113A21, which has a rise time of $\leq 1\mu$s. The second source is the uncertainty in determining when the shock arrives from the pressure trace. Figure 22 and 23 below display two examples of raw data displaying the shock arrival pressure trace.

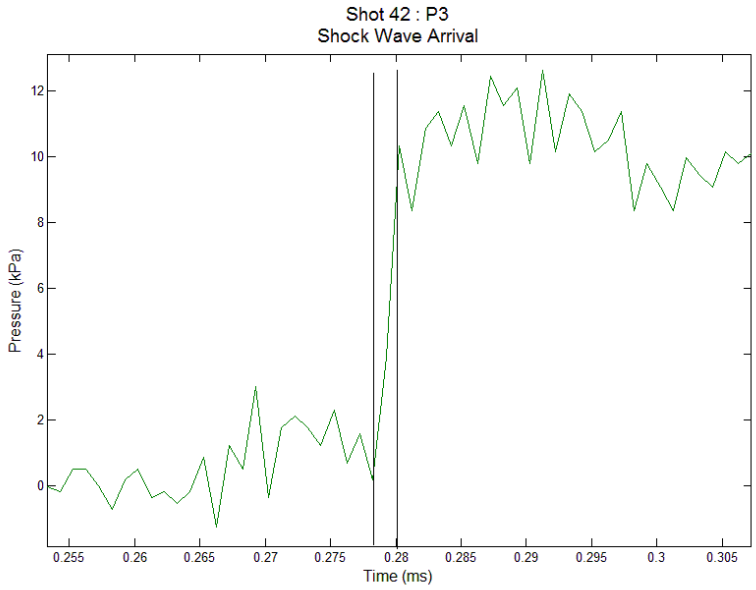

Figure 22: Clean Shock wave arrival.

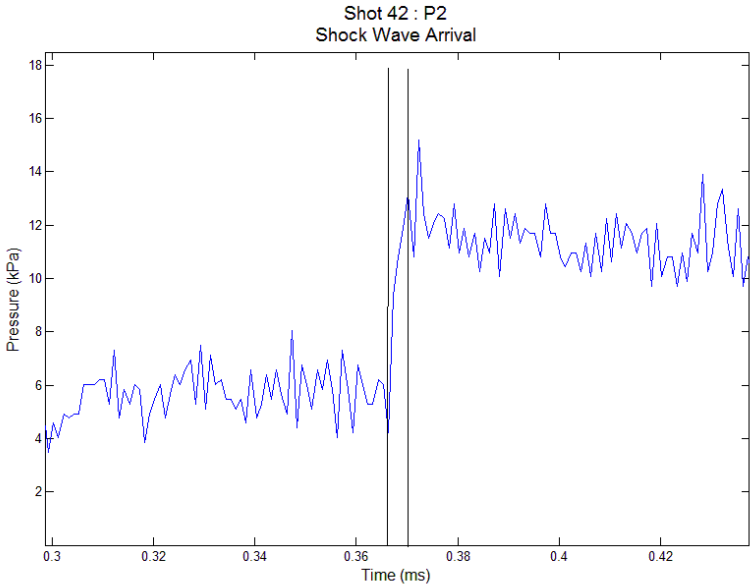

Figure 23: Less clear shock wave arrival.

These figures demonstrate that the shock arrival is not uniform between pressure measurements and may take muliple μs. The average time accross the shock from all all tests, excluding the one combustion run, is calculated to be 3.2μs. The combustion run is excluded because the time resolution is much less than the other runs. Since the shock arrive is within this time frame, the uncertainty indetermining when the shock arrives will assumed to be half this value. Combining this uncertianty with the pressure transducer rise time, the $\delta t_m = 2.6\mu$s. The average time of the shock between pressure transducers, which is used to determine shock velocity, is 159μs and the average distance between the transducers is 0.254 m. Therefore the approximate percent uncertainty in shock velocity is calculated to be 1.6%.

6.2 Pressure jump

Regarding the pressure jump across the shock, only one pressure transducer trace is required. The pressure jump is calculated through subtracting the pressure after the jump, $p_{a,n}$, from before the jump,$p_{b,n}$, 14. Therefore the uncertainty in this measurement is twice the uncertainty in the pressure measurements.

$$\delta p_n = \delta p_{a,n} + \delta p_{b,n} \tag{14}$$

While the raw data was used to determine shock arrival times, the noise in the data made it advantagious to uses averaging before determining the pressure values. For this, multiple average techniques were attemped, but the best method was determined to be averaged each point with its two adjacent points. In this paper, this is referred to as $N = 3$ averaging. This removed a portion of the noise without removing larger physical fluctuations in the data. This was was the best way to determine the pressure imediatly after the shock. The noise in the data was determined from pressure reading recorded before the diaphram was ruptured. An approximate magnitude of the noise was determined from each shot for the raw and $N = 3$ averaged data. Accross all runs, the average noise in the raw data has an amplitude of 0.461 kPa with a standard deviation of 0.163 kPa, while the averaged data has an amplitude of 0.220 kPa with a standard deviation of 0.066 kPa. The averaged data reduced the noise by about half.

In addition to noise in the data, there are many other fluctuations. These come from both electrical and pressure effects. The electrical affects are believed to be due to the burster. Though the shock tube is adequatly grounded, the electrical discharge coming from the burster creates a larger decaying oscilation at

the time the burster is fired. This caries over into the pressure reading of the shock arrival frequently for location $m = 4$ since the shock arrives there first. An example of this is provided in figure 24.

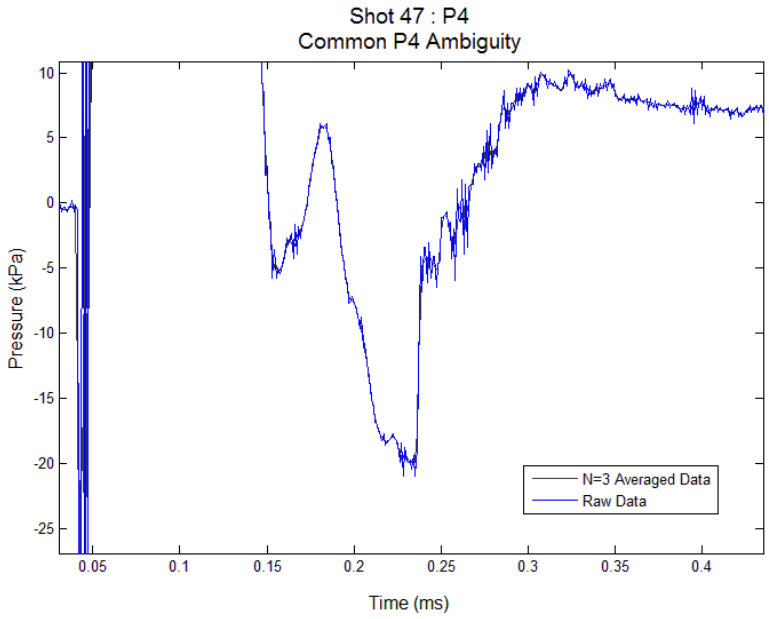

Figure 24: Burster discharge effect on pressure reading.

Here, the shock location may be determined, however, determining the pressure jump will be inaccurate because of the other effects. The effect of the burster is usually gone by $m = 3$. Additionally, there are other fluctuations besides the burster effects. Figure 25 is a representative case of these distinct oscillations in the data.

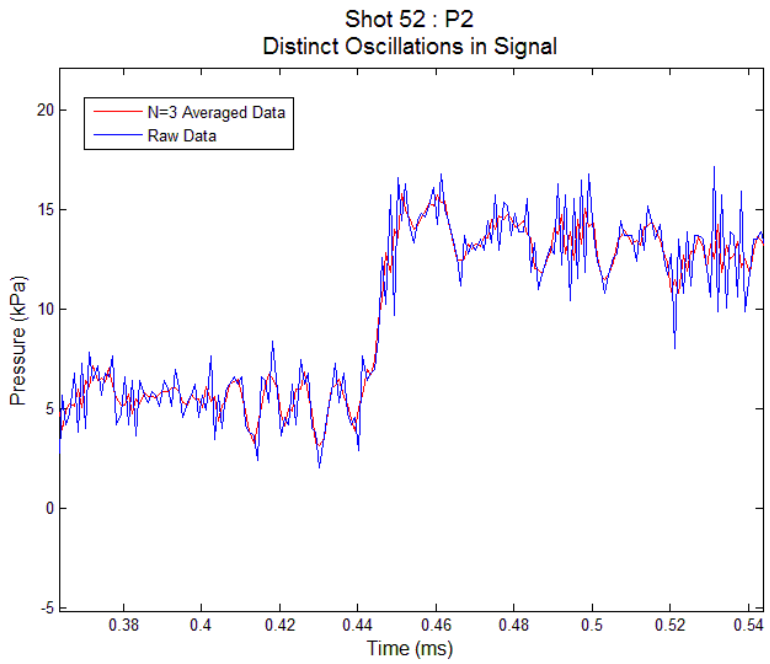

Figure 25: Raw and averaged data displaying distinct oscillations.

The origin of these oscillations may be from from boundary layer effects. This would explain the oscillations after the shock, but not before. These may be other electrical or from vibrations in the pipe. Using the example above the magnitude of the oscillations in kPa are as follows: raw data before shock 4.39, after shock 3.29 and averaged data before shock 2.561, and after shock 1.77. Much effort was placed in using Fourier transforms and locating these frequencies in order to remove them. It was found that while these frequencies and corresponding oscillations may be removed, it did not aid in determining shock location or pressure jump. It did not aid in determining the shock arrival time because it is clear before the frequencies are removed. It did not aid in determining the pressure jump because removing the frequencies changed the magnitude of the pressure reading. Therefore, an accurate pressure jump reading could not be made. After this analysis, it was determined that only $N = 3$ averaging would be used.

Therefore, to determine $\delta p_{a,n} + \delta p_{b,n}$, two approaches may be taken. The average magnitude of the noise may be used, or the magnitude of the oscillations found in each signal. If the first is used with the averaged data, $\delta p_n = 0.44$ kPa. If the second is used with the averaged data, taking shot 52, $p2$ as an example $\delta p_n = 2.16$ kPa with $\frac{\delta p_2}{p_2} = 24.6\%$. The second method has a much larger δp_n, which is more in line with the deviation of the experimental results from the predicted. MATLAB routines used for Fourier analysis and averaging can be found in appendix B

7 Results

7.1 Data Selection

Due to the noise in the raw and averaged data, there was often ambiguity in determining the points before and after the arrival of the shock for velocity and pressure readings. Figure 25 displays an example of this difficulty. Therefore, to select the velocity and pressure data, the time points before and after the arrival of the shock were chosen to be the point just before an obvious pressure change not due to noise was pressent. Then, referencing these points, the pressure points, using the $n = 3$ averaged data, were chosen to be the point immediatly precending the time reading for before the shock, and immediatly following the time

reading for just after the shock. It was attempted to remain consistent as possible. However, in situations were these points were obviously not the best, other time and pressure readings were used.

Figure 26 pictorially represents the general procedure for how the time between incident shock arrival and the pressure jump across the incident shock were obtained.

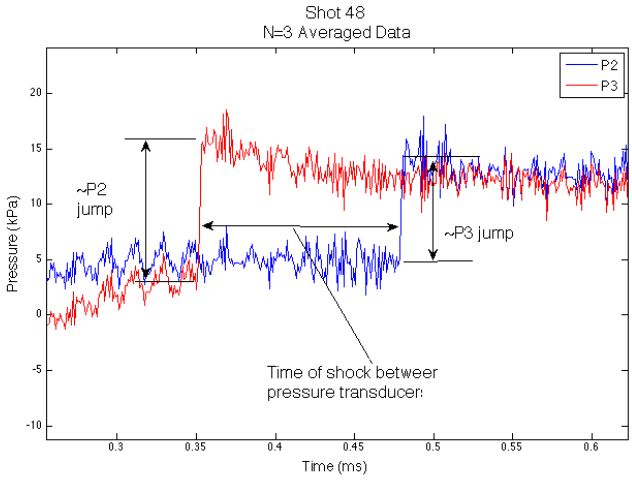

Figure 26: General procedure for extraction of the incident shock data

7.2 Exclusion of $p4$

The pressure reading at $m = 4$ often had other anomalies in the shock pressure reading. These are mostly likely a result of lingering electrical discharge resulting from the diaphragm burster, but could also be caused by non-ideal diaphram rupture and since this pressure reading is closest to the diaphram, the shock may not have yet coalesced. An example of this is provided in figure 27 below. Note that $p4$ here is the pressure read by transducer $m = 4$, not the pressure in the driver section used in the shock tube equation, denoted p_4.

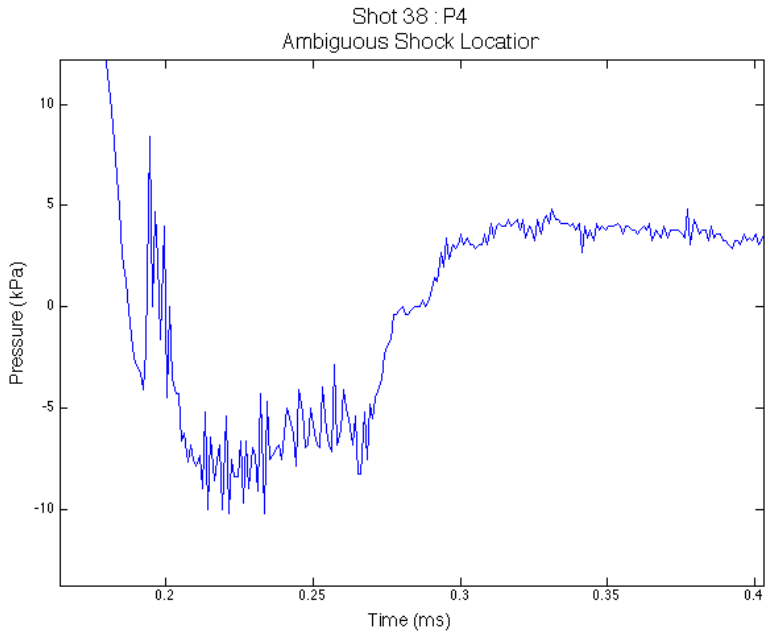

Figure 27: $p4$ shock behavior possibly due to non-ideal diaphram rupture.

These were determined to be sufficients reason to exclude all $p4$ pressure readings from calculations and results presented in figure 28 and figure 29.

7.3 Combined Data

In figures 28 and 29 and in appendix D, the combined experimental and predicted results are presented.

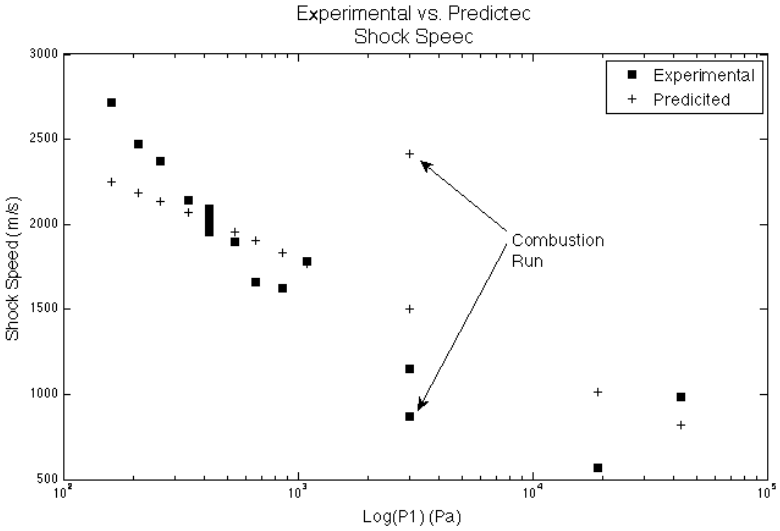

Figure 28: Compilation of experimental and predicted shock speeds based on initial driven pressure.

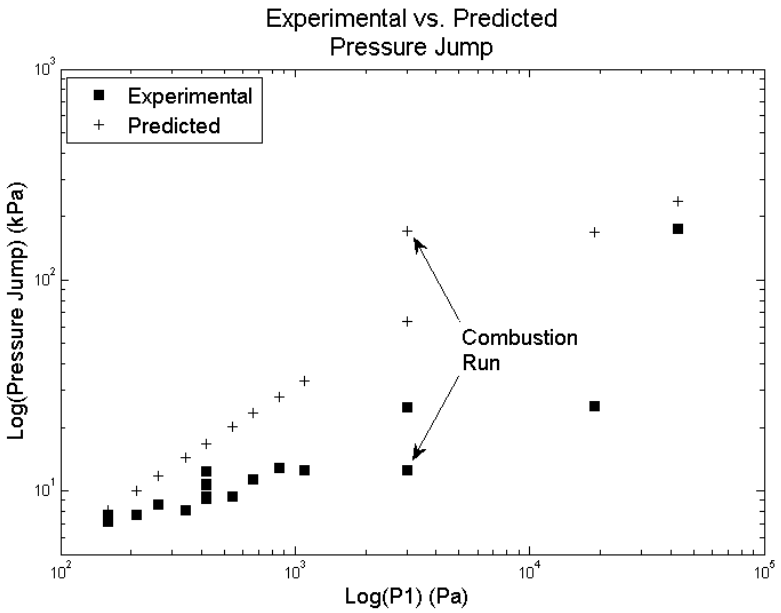

Figure 29: Compilation of experimental and predicted shock speeds based on initial driven pressure.

The average percent error in the shock speed is 2.7% with a standard deviation of 12.04%. The average percent error in the pressure jump is −37.5% with a standard deviation of 16.8%. As seen in the plot, the combustion run had a much higher error than the average error for both the shock speed and pressure jump. Since the pressure jumps in figure 29 are on average less than the predicted value, the percent error in pressure jump was recalculated for each pressure transducer across all runs. The data is gathered in table 3. For this calculation, shots 56 and 1000 were exluded because of their large percent errors.

$p_2 - p_1$ Percent Error per Transducer		
n	Average	Standard Dev
1.00	-49.49	13.90325249
2.00	-42.71	12.49519488
3.00	-22.80	25.6588771
4.00	-5.19	22.93614769

Table 3: Average pressure jump percent error for each pressure transducer

Though pressure transducer $p4$ had more sources of noise in the data and less coalesced shocks, it had the lowest percent error. Even though the pressure jumps at $p4$ were the greatest of all the pressure transducers, the measurements were still below the prediction. Additionally, using the local shock speed, each V_n, the expected pressure rise using normal shock relations was calculated from equation 3.

This was to investigate if the non-ideal opperation was due to the burster, but ideal operation regained as the shock wave traveled down the tube. However, the perecent error between measured pressure jump, averaged over the two transducers used to make a velocity calculation, had a percent error of -20.7% and a standard deviation of 22.2%. This is an improvement over the percent errors in figure 29, but still very large.

Just as with the pressure jump, the percent error in velocity measurement across each pressure transducer pair was calcuated. The results are presented in table 4. For $n = 3$, the first pair of transducers from the diaphram, the shock speed is faster than predicted on average. As it travels down the tube, it slows so that by the last pair, it is slower than predicted on average. Again, shots 56 and 1000 were excluded because of

their large percent errors.

u_s Percent Error per Transducer Pair		
m	Average	Standard Dev
1	-3.03	11.23543254
2	8.23	13.27543939
3	19.83	15.46953315

Table 4: Average shock speed percent error for each pressure transducer pair.

To help visualize these results, two x-t diagrams are provided using data from shot 38 and shot 53 in figures 30 and 31 below. The exact time the diaphram ruptures is not known. Therefore, while the time between each of the experimental points has been measured, their exact position on the time scale is not known. They have been positioned close to the predicted line, but this position is not from measurments. Only the slope of the data points should be compared with the theoretical line. It is interesting to note that the data for both shots show a decreasing shock speed along the length of the tube, but shot 38 at Mach 8.3 has a higher initial shock speed than predicted by theory while shot 53 at Mach 3.45 has about the same initial shock speed as predicted.

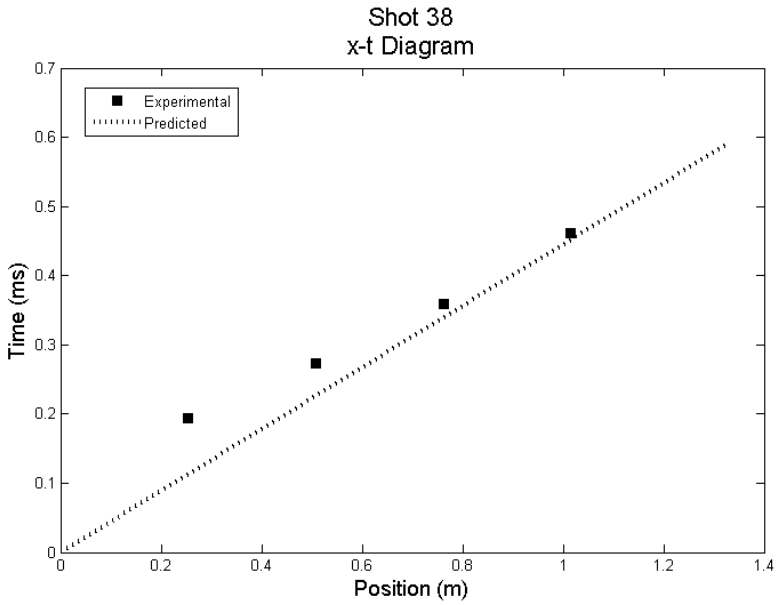

Figure 30: X-t diagram for shot 38.

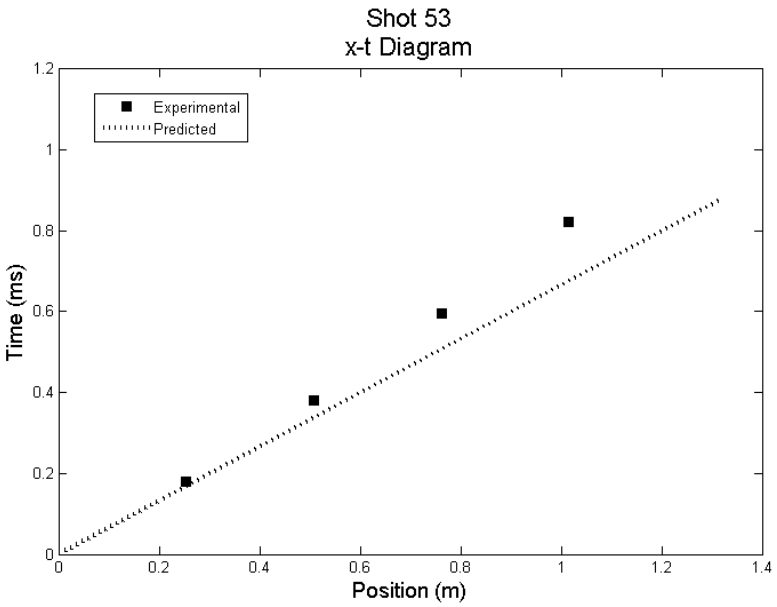

Figure 31: X-t diagram for shot 53.

Figures 32 and 33 represent an alternative method of visualizing the data. Instead of plotting the results in $x-t$ space, the results are plotted in terms of velocity and pressure, as indicated in the figures. Errors present in the $x-t$ diagrams manifest in the $p-u$ diagrams as well. The red and blue curves are the result of solving equations 3, 4, and 2 for the velocity of the contact surface. $\frac{p_4}{p_1}$ is used along with the gas properties to calculate these curves.

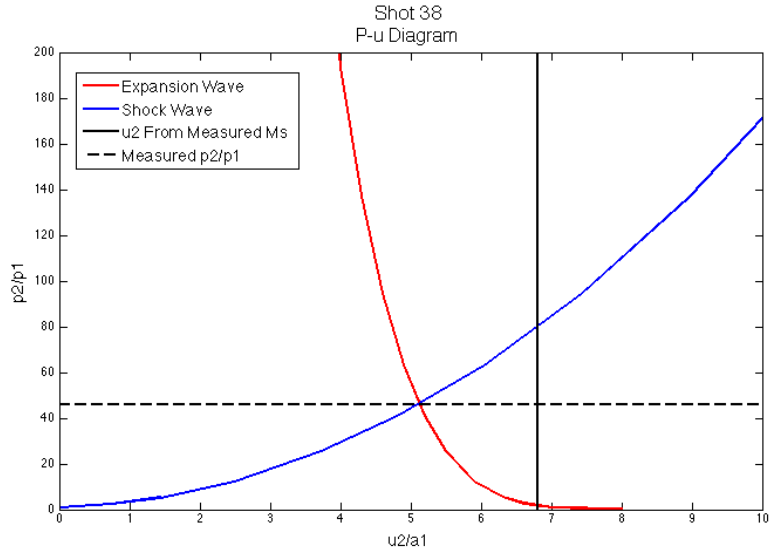

Figure 32: p-u diagram for shot 38.

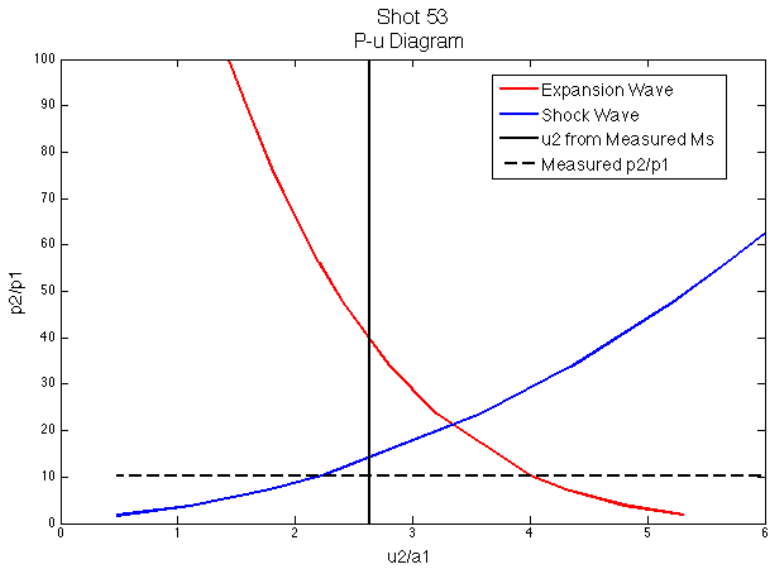

Figure 33: p-u diagram for shot 53.

8 Discussion

A large volume of data exists for the helium shots performed in the shock tube, allowing for a great deal of analysis and comparison to the predictions made by Cantera. On average fairly good agreement (at most 20% difference, more often much less) exists between the data and predictions for the speed of the incident shock. Shock speed measurements between the individual transducers, however, revealed some disagreement that can be attributed to non-ideal effects.

In every case the incident shock is observed to decelerate as it propagates down the length of the driven section. In shots with lower values for $\frac{p_4}{p_1}$, on the order of about 300, the measurements closest to the diaphragm agree very closely to the predicted values for shock speed, but the measured speed decreases as the shock propagates toward the end of the tube. A similar phenomenon is observed for shocks with pressure ratios on the order of 3000-4000, but the initial speed measurement in those cases is higher than predicted by theory and the shock is slowed to a speed that is typically just below the predicted value. Since the measurement uncertainty is only about 1.6% as seen in section 6, this decrease in shock speed is a physical occurrence and not a systematic error in the system.

The effect of a shock being slowed or attenuated as it propagates down the length of a shock tube has been well-documented in the literature. It is explained quite well by Mirels. The gas in region 2 between the incident shock and the contact surface is moving rapidly in driven section, and boundary layers exist in this region near the walls of the tube. The thickness of the boundary layers grows as the gas propagates unsteadily, and therefore the boundary layers must absorb mass from the high-speed region in the center of the tube as they grow. This absorption causes the boundary layers to act as "aerodynamic sinks,", simultaneously accelerating the contact surface and decelerating the incident shock until an equilibrium is reached [7]. This effect very well explains the attenuation of the shock observed in experimental data.

Since the very small systematic error in the shock speed measurements does not account for the substantial differences in shock speed observed, it follows that the incident shock speed being higher than predicted by theory in the first measurements made must be a physical effect as well. The cause of this effect is more subtle than the previous one described, but the effect itself is also well-documented. Gaydon reports that White (1958) was among the first to report this phenomena. It is attributed partly to non-ideal diaphragm removal, in that in high $\frac{p_4}{p_1}$ situations the incident shock is formed by a series of compression and expansion

waves, extracting more energy from the driver gas than predicted by ideal-diaphragm removal. There is an additional contribution to the observed higher initial shock speed, namely the abrupt area change between the two sections of the tube at the diaphragm. The resulting increase in shock performance was studied by Resler et al in 1952. Both of these effects have a strong dependence on $\frac{p_4}{p_1}$, and are in fact not observable at values below 1000 [5]. In combination, they very neatly explain the behavior exhibited in the data.

Experimental data for the pressure jump across the incident shock, however, is consistently much lower than the values predicted by theory. It is also observed from the data that the pressure jump across the shock decreases as the shock propagates. The second effect can be explained by the attenuation of the shock since from equation 3 it is apparent that the pressure jump across the incident shock is dependent on M_s^2. The fact that almost all of the pressure readings are substantially lower than predicted is somewhat more difficult to explain. It is postulated that the protective coating of RTV applied to the pressure transducers to protect them from the high temperature gases in the tube could be affecting the pressure readings, which would require a recalibration of each transducer.

A qualitative effort can be made to explain the less-than-ideal results of attempting combustion shots. The only differences between the successful shots of Bélanger and the unsuccessful ones in this experiment are the fact that the driver gases are now fully mixed and the initial pressure in the driver section is much lower. Pre-mixing of the driver gases certainly should not account for the lower reaction rate observed, so the pressure should be the cause.

Tse et al reports that for a mixture of hydrogen, oxygen, and helium mixed in the ratio used in this experiment, pressure has an inconsequential effect on the flame speed [3], as can be observed from figure 34.

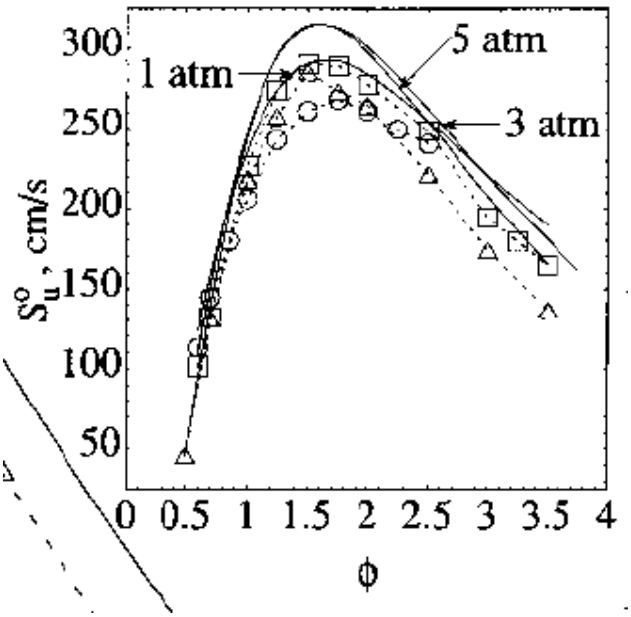

Figure 34: Measured and calculated unstretched laminar burning rates as a function of equivalence ratio for H_2/O_2/He flames at 1, 3, and 5 atm where % He = 70% at ϕ=1

This would seem to suggest that pressure would not affect the flame speed, but it can have a strong influence on the effective surface area for turbulent reactions in instances where the combuster geometry is complex such as the one in this experiment [1]. Lower pressure is therefore very likely the culprit for the poor performance observed in combustion shot attempts.

Several routes for future work are possible. First, the shock tube could be moved into a combustion laboratory where it could then be operated at full scale, as was originally intended. This would be the best solution for reproducing Bélanger's results, but it would involve a great deal of effort. A second option

is to decrease the amount of helium in the mixture in the driver. An increased amount of hydrogen and oxygen would certainly speed up the reaction and give results much closer to the constant internal energy calculations performed by Cantera. A final option would be to combust the hydrogen in air instead of a mixture of oxygen and helium. Nitrogen has a lower thermal conductivity than hydrogen, about five times smaller, which would allow for a faster reaction since the high temperatures created by combustion would remain concentrated in the reaction zone, sustaining a higher overall temperature and speeding the reaction.

9 Conclusion

The purpose of this study was to build a combustion driven shock tube and perform tests and compare with theory for high Mach numbers. The combustion driven shock tube was built and tested with Helium at high Mach numbers. The experimental results verify proper functioning of the shock tube, but show significant deviation between experimental results and ideal theory. This deviation was greater for the pressure jump than velocity measurements, and the deviations in velocity measurements are explained through well-documented physical phenomena. Due to various safety concerns, the original combustion test matrix was not able to be completed. The safety concerns limited the driver fill pressure to 1 bar, from a previously planned 20 bar. The only combustion run completed had an appreciably slower burn rate than ones performed by Bélanger at higher pressures. This caused more heat loss and therefore lower driver pressure. Because of this, the diaphram did not rupture completely, making the shock weaker than with a proper rupture. In order to perform combustion runs, either fill pressure must be increased or the mixture must be changed via either a lower concentration of helium or combusting hydrogen in air. With these changes, experiments with the combustion driven shock tube can be performed as originally planned.

10 Acknowledgements

The authors of this report would like to thank individuals who greatly assisted with multiple phases of this project. The authors would like to thank Professor Joseph Shepherd and Nicholaus Parziale for continued guidance, suggestions, and impetus for the project. The authors would also like to thank Philip Boettcher and Jason Damazo for their assistance and suggestions. Finally, the authors would like to thank Rémy Mevel for allowing use of his experimental apparatus.

References

[1] Conversation with Professor Joseph Shepherd, June 2012.

[2] Jacques Bélanger. *Studies of Mixing and Combustion in Hypervelocity Flows with Hot Hydrogen Injection*. PhD thesis, California Institute of Technology, April 1993.

[3] The Combustion Institute. *Morphology and Burning Rates of Expanding Spherical Flames in H_2/O_2/Inert Mixtures Up to 60 Atmospheres*, volume 28, 2000.

[4] Jason Damazo. Galcit 6-inch shock tube handout. Ae 104b, 2011.

[5] A.G. Gaydon and I.R. Hurle. *The Shock Tube in High-Temperature Chemical Physics*. Reinhold Publishing Corporation, 1963.

[6] Göran S. Holmstedt. The upper limit of flammability of hydrogen in air, oxygen, and oxygen-inert mixtures at elevated pressures. *Combustion and Flame*, 17:295–301, 1971.

[7] Harold Mirels. Shock tube test time limitation due to turbulent wall boundary layer. Technical Report 405843, Aerodynamics and Propulsion Research Laboratory, May 1963.

[8] Bradford Sturtevant. Ae 101 notes. California Institute of Technology, April 2001.

Appendices

A CAD Drawings

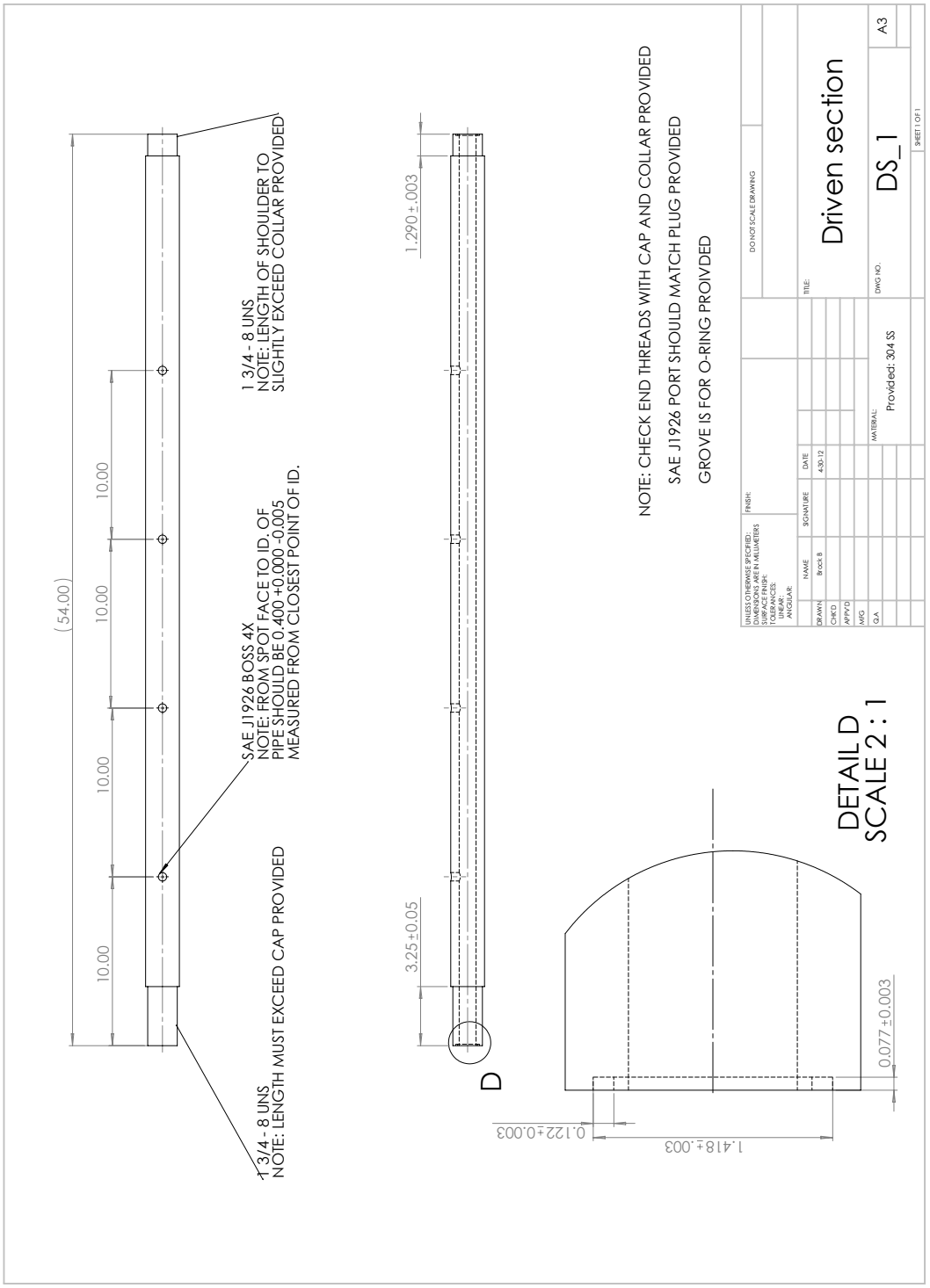

Figure 35: Driven Section

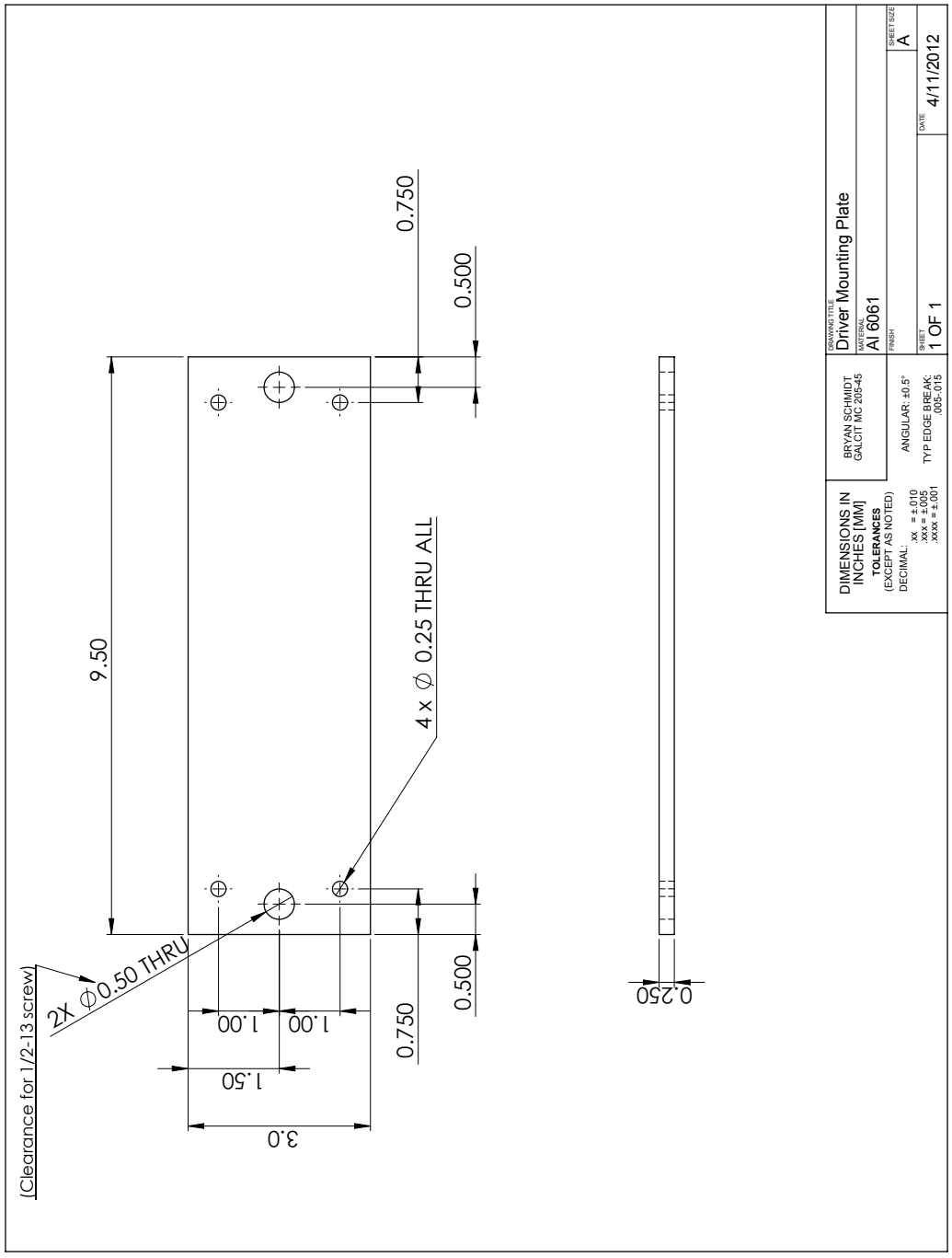

Figure 36: Mounting plate for driver section

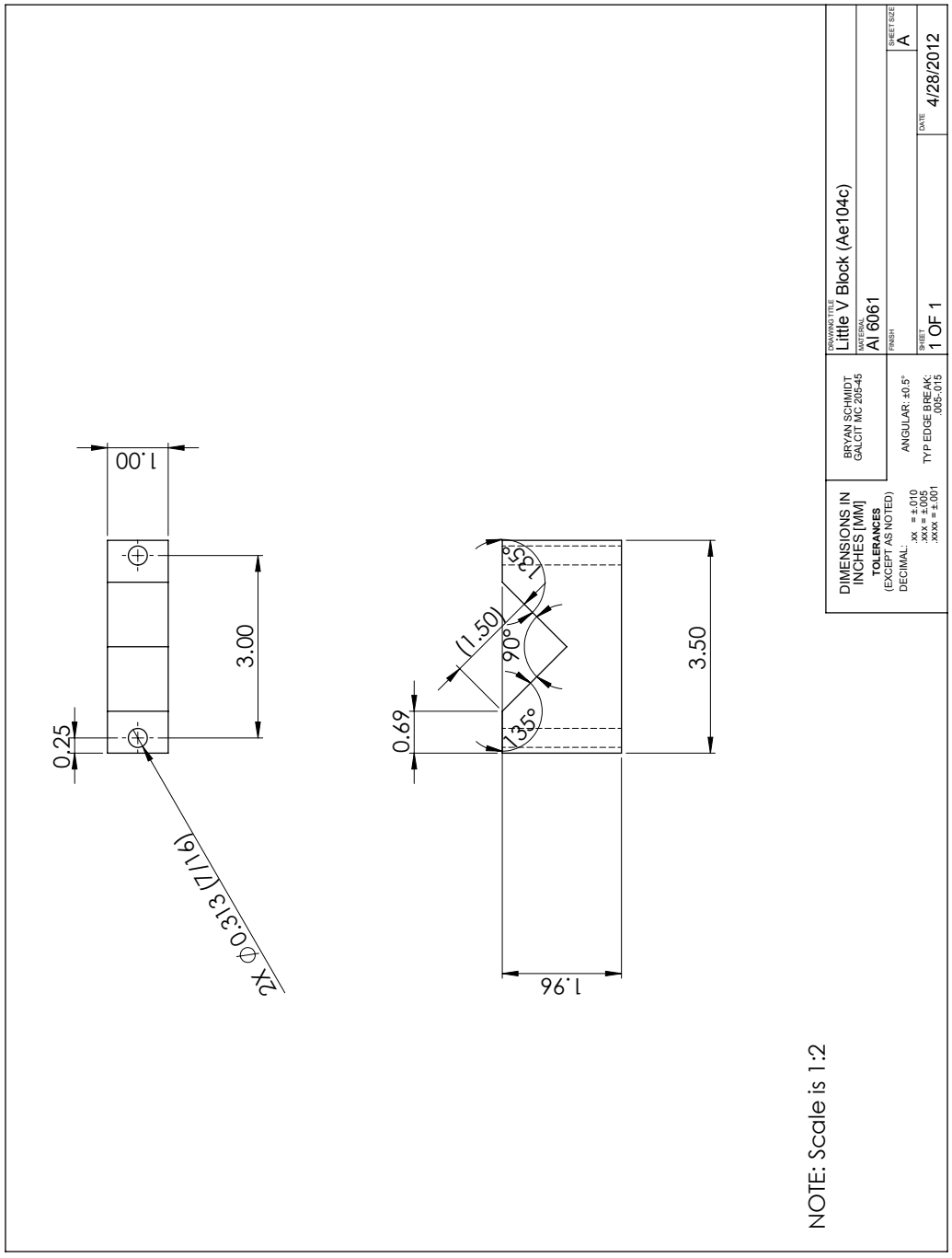

Figure 37: Driven section V-block

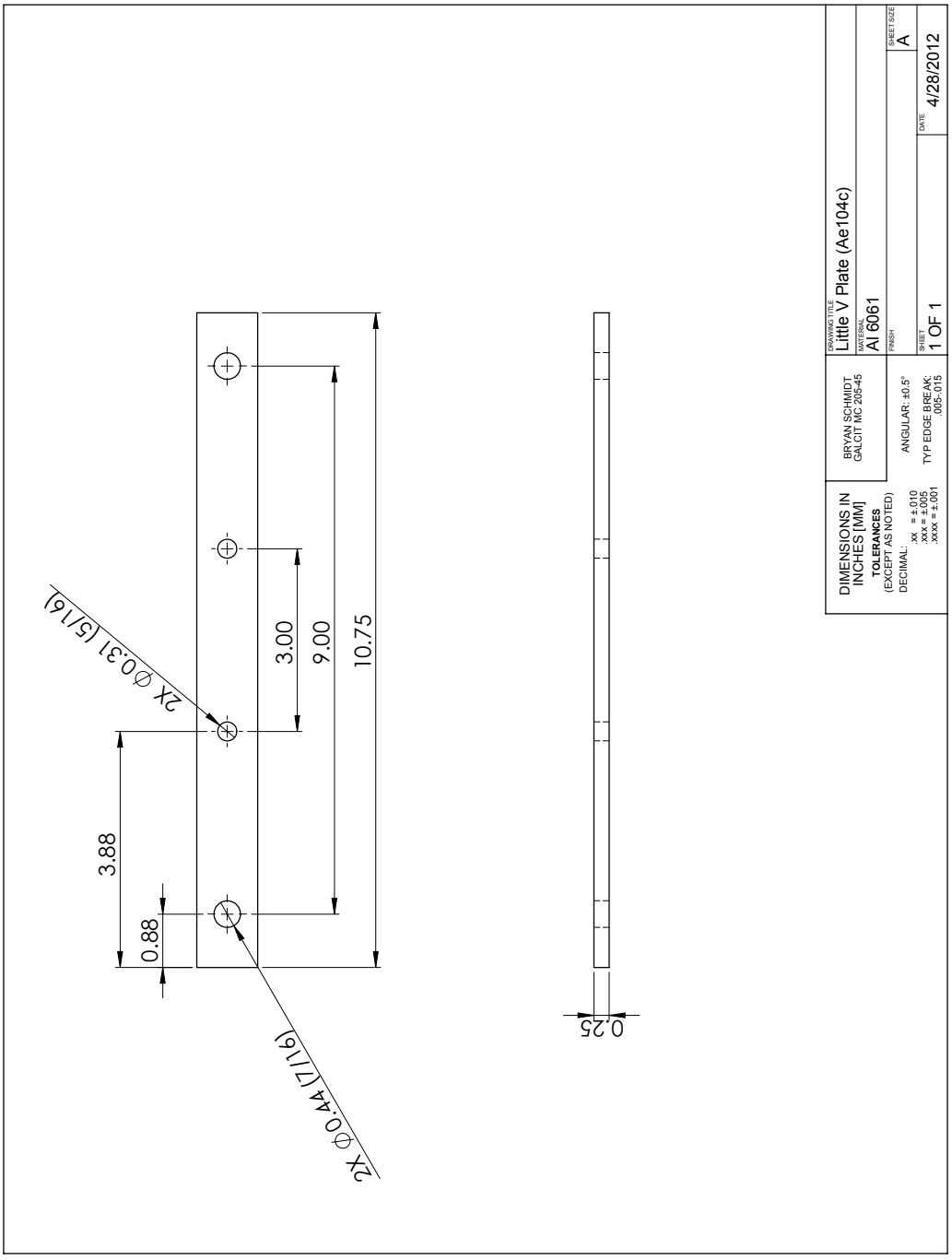

Figure 38: Mounting plate for driven section V-block

B MATLAB Scripts

6/5/12 11:37 PM /Users.../NI_DAS_6133_combustion_driver.m 1 of 3

```
clc
clear all
%close all


if (~isempty(daqfind))
    stop(daqfind)
end

% duration and pretrig in milliseconds
Duration = 300;
PreTrig = 50;
% sample rate in Hz
SR = 20e3;
% trigh value in volts


trigger_val = 1.0;


% shot number
shot = 1000;


% warn the user if shot data already exists
shotExists = exist(['shot' num2str(shot)],'file');
if shotExists ==7
    fprintf('Warning! Data for This Shot Already Exists!\n')
    reply = input('Do You Want to Overwite the Data? Y/N [Y]: ', 's');
    if reply == 'N'
        break
    elseif reply == 'n'
        break
    else
    end
else
end



Duration = Duration/1000;
PreTrig = PreTrig/1000;







fprintf('Starting to load the settings to Card(s)\n')

% make new objects
AI1 = analoginput('nidaq','Dev4');



% add channels to both objects
ch1 =  addchannel(AI1,1:7);

% name the trigger channel, call it the first channel in for both devices
triggerChannel1 = addchannel(AI1, 0);

% make a scalegoogl
scale1 = [- 5,5];

% set the input type. this must match what is on the breakout box itself
```


Figure 39: Routine used for DAS (Page 1 of 3)

```
set(AI1,'InputType','Differential')

fprintf('Loading the Aquisition Settings\n')
% manipulate the aqusition settings, this must be done for each card
set(AI1.Channel(1:7), 'SensorRange', scale1);
set(AI1.Channel(1:7), 'InputRange', scale1);
set(AI1.Channel(1:7), 'UnitsRange', scale1);
set(AI1.Channel(1:7), 'Units', 'Volts');



fprintf('Loading the Sampling Rates\n')
% set the sampling rate for each card, the find the actual SR
set(AI1,'SampleRate',SR)
ActualRate1 = get(AI1,'SampleRate');
set(AI1,'SamplesPerTrigger',Duration*ActualRate1)
blocksize1 = get(AI1,'SamplesPerTrigger');
Fs1 = ActualRate1;



fprintf('Loading the Trigger Settings\n')
% set the trigger setting for each card
set(AI1,'TriggerChannel',triggerChannel1)
set(AI1,'TriggerType','Software')
set(AI1,'TriggerCondition','Rising')
set(AI1,'TriggerConditionValue',trigger_val)
set(AI1, 'TriggerDelayUnits', 'Samples');
set(AI1, 'TriggerDelay', -PreTrig*ActualRate1);


fprintf('Arming\n')


%%

% actually arm the two cards
start(AI1)
fprintf('Armed\n')

%%
wait(AI1,10^100)

fprintf('Triggered\n')
data1 = getdata(AI1);



delete(AI1)
clear AI1


fprintf('Writing the Time Array and Organizing the Data\n')
t = linspace(-PreTrig,Duration-PreTrig,blocksize1);
t = t';

data = [data1(:,1:end)];
trigdata = [data1(:,end)];

fprintf('Saving the Aquired Data\n')
dataStruct = [t data];
num2str(shot);
mkdir(['shot_' num2str(shot)])
save(['shot_' num2str(shot) '\shot_' num2str(shot) '_combustion_driver_data.txt'],↵
'dataStruct', '-ASCII');
save(['shot_' num2str(shot) '\shot_' num2str(shot) '_combustion_driver_data.mat'],↵
'dataStruct');
makeSenseKey(shot)
```

Figure 40: Routine used for DAS (Page 2 of 3)

```
%%
fprintf('Plotting the Aquired Data\n')

figure(2)
plot(t*1000,data*1e3)
legend('1','2','3','4','5','6','7','8','9','10','11')
xlabel('Time (ms)')
ylabel('Potential (mV)')
grid on
```

Figure 41: Routine used for DAS (Page 3 of 3)

```
clc; clear all;

setCanteraPath

Ru = 8.314472e3; %universal gas constant
p1   = 420;   %pressure in the driven section
%% calcualte the conditions in the combustion driver
T4i = 300;     %the driver starts at RT
% p4i = 500;  %use this to convert to psi if you want
% p4i = p4i/0.00014503773801;
p4i = 25e3;  %initial pressure in the driver section in kPa

% gas4 = importPhase('h2o2he_6000k.cti');  %use shep,s mech for air
gas4 = gri30;

% Hydrogen partial pressure in the driver, then say half that is O2 by
% stoichiometry

ph2 = 29.6/100;
po2 = ph2/2;
phe = 1-ph2-po2;
concentrationString = ['H2:' num2str(ph2) ',O2:' num2str(po2) ',N2:' num2str(phe) ];

mw4 = molecularWeights(gas4);
nsp = nSpecies(gas4);
set(gas4,'T',T4i,'P',p4i,'X',concentrationString);
equilibrate(gas4,'UV');
mw4 = meanMolecularWeight(gas4);
R4 = Ru./mw4;
T4 = temperature(gas4);
g4 = cp_mass(gas4)/cv_mass(gas4);
p4 = pressure(gas4);


%% predict the shock speed and setup problem

g1   = 1.4;

T1   = 297;
R1   = 287.0028;

a1   = sqrt(g1*R1*T1);
a4   = sqrt(g4*R4*T4);

r1     = p1/(R1*T1);
r4     = p4/(R4*T4);

u1     = 0;
u4     = 0;

% guess

p2   = p1*10;
p3   = p1*10;
u2   = 3e3;
u3   = 3e3;
Ms   = 11;

x01 = [p2,p3,u2,u3,Ms];

%% solve for the values behind the initial shock
options=optimset('Display','iter','MaxFunEvals',100000,'MaxIter',100000,'FunValCheck',↵
'on','TolFun',1e-1000,'TolX',1e-1000);%,'PlotFcns',@optimplotfval);   % Option to↵
display output
% options=optimset('MaxFunEvals',100000,'MaxIter',100000,'FunValCheck', 'on','TolFun',↵
1e-100,'TolX',1e-100);%,'PlotFcns',@optimplotfval);   % Option to display output
[x1,fval] = fsolve(@shockFrozenDriver,x01,options,g1,T1,p1,R1,gas4,u1,u4);  % Call↵
solver
```

Figure 42: Routine used to model shock tube with Cantera (Page 1 of 3)

```
%%
p2     = x1(1);
p3     = x1(2);
u2     = x1(3);
u3     = x1(4);
Ms1     = x1(5);
usP     = Ms1*a1;

T3     = T4*(p3/p4)^((g4-1)/g4);
r3     = r4*(p3/p4)^((1)/g4);
a3     = sqrt(g4*R4*T3);

T2     = T1*(1+2*(g1-1)/(g1+1)^2*(Ms1.^2-1).*(1+g1*Ms1.^2)./Ms1.^2);
r2     = r1*Ms1^2/(1+(g1-1)/(g1+1)*(Ms1^2-1));
a2     = sqrt(g1*R1*T2);


P1 = p1;
us1 = usP*1;   % fudge factor for T5 (our ST is too long) is yours?
%% Use canterra to find the conditions after the initial shock using an estimate of the
shock speed

q = 'O2:0.209796 N2:0.780880 AR:0.009324';   %this is air, might have to add h20
initially if humid day
% mech = 'gri30_highT.cti';
% mech = 'airNASA9.cti';
mech = 'n2-o2-e_highT.cti';


gas1 = importPhase(mech);
set(gas1, 'T', T1, 'P', p1, 'X', q);
gas2 = importPhase(mech);
set(gas2, 'T', T1, 'P', p1, 'X', q);
gas5 = importPhase(mech);
set(gas5, 'T', T1, 'P', p1, 'X', q);


[gas2] = PostShock_eq(us1, p1, T1, q, mech);
g2 = cp_mass(gas2)/cv_mass(gas2);
T2 = temperature(gas2);
p2 = pressure(gas2);
r1 = density(gas1);
r2 = density(gas2);
u2 = us1-r1*us1/r2;
R2 = Ru./meanMolecularWeight(gas2);
s2 = entropy_mass(gas2);
q2 = moleFractions(gas2);


[p5,ur1,gas5] = reflected_eq(gas1,gas2,gas5,us1)
g5 = cp_mass(gas5)/cv_mass(gas5);
T5 = temperature(gas5);
p5 = pressure(gas5);
r5 = density(gas5);
R5 = Ru./meanMolecularWeight(gas5);
s5 = entropy_mass(gas5);
q5 = moleFractions(gas5);

%%
disp(' ')
disp('Conditions for Combustion Driver')
disp(['p4iHe    = ' num2str(round(p4i*phe/10^3*100)/100) '   [kPa] '  num2str(round
(p4i*phe/10^3*100*7.50061683)/100) '  [Torr] '  num2str(round(p4i*phe/10^3*100*0.
145037738)/100) '  [Psi]'])
disp(['p4iH2    = ' num2str(round(p4i*ph2/10^3*100)/100) '    [kPa] '  num2str(round
(p4i*ph2/10^3*100*7.50061683)/100) '  [Torr]  '  num2str(round(p4i*ph2/10^3*100*0.
145037738)/100) '  [Psi]'])
disp(['p4iO2    = ' num2str(round(p4i*po2/10^3*100)/100) '     [kPa] '  num2str(round
```

Figure 43: Routine used to model shock tube with Cantera (Page 2 of 3)

```
(p4i*po2/10^3*100*7.50061683)/100) '  [Torr]    '  num2str(round(p4i*po2/10^3*100*0.↵
145037738)/100) '  [Psi]'])
disp(['p4i       = ' num2str(round(p4i/10^3*100)/100) '   [kPa] '  num2str(round↵
(p4i/10^3*100*7.50061683)/100) '  [Torr]    '  num2str(round(p4i/10^3*100*0.145037738)↵
/100) '  [Psi]'])

% disp(['p4i       = ' num2str(round(p4i/10^6*100)/100) '   [MPa]'])
disp(['T4i       = ' num2str(round(T4i)) '    [K]'])
disp(['p4        = ' num2str(round(p4/10^3*100)/100) '   [kPa]    ' num2str(round↵
(p4/10^3*100*0.145037738)/100) '  [Psi]'])
disp(['T4        = ' num2str(round(T4)) '    [K]'])
disp(' ')
disp('Conditions behind Incident Shock')
disp(['p2        = ' num2str(round(p2/10^3*100)/100) '   [kPa]    ' num2str(round↵
(p2/10^3*100*0.145037738)/100) '  [Psi]'])
disp(['T2        = ' num2str(round(T2)) '    [K]'])
disp(['r2        = ' num2str(round(r2*100)/100) '   [kg m^-3]'])
disp(['u2        = ' num2str(round(u2)) '    [m s^-1]'])
disp(['us        = ' num2str(round(us1)) '    [m s^-1]'])
disp(['Ms        = ' num2str(round(us1/a1*100)/100) '   '])
disp(' ')
disp('Conditions behind Reflected Shock')
disp(['p5        = ' num2str(round(p5/10^3*100)/100) '   [kPa]    ' num2str(round↵
(p5/10^3*100*0.145037738)/100) '  [Psi]'])
disp(['T5        = ' num2str(round(T5)) '    [K]'])
disp(['r5        = ' num2str(round(r5*100)/100) '   [kg m^-3]'])
disp(['ur        = ' num2str(round(ur1)) '    [m s^-1]'])
disp(' ')
```

Figure 44: Routine used to model shock tube with Cantera (Page 3 of 3)

```
load('shot_52_combustion_driver_data.mat'); %Loads shot data in a variable
called "dataStruct"
load('shot_52_combustion_driver_sensitivity.mat'); %Loads all settings
t=dataStruct(:,1)*1e3; %Time variable, convert to ms
%The following load in pressure readings, converting from voltage to
%pressure in kPa
p1=dataStruct(:,3)*1e3/cell2mat(sens(3));
p2=dataStruct(:,4)*1e3/cell2mat(sens(4));
p3=dataStruct(:,5)*1e3/cell2mat(sens(5));
p4=dataStruct(:,6)*1e3/cell2mat(sens(6));
pend=dataStruct(:,2)*1e3/cell2mat(sens(2));
plot(t,p1,t,p2,t,p3,t,p4,t,pend)
title(['Shot Number ',num2str(cell2mat(shotCell(2)))])
legend('P_1','P_2','P_3','P_4','P_{endwall}')
xlabel('Time (ms)')
ylabel('Pressure (kPa)')


%% Average Section
%# of points to average
n=3;
%measurement to change
p=p1;
avp1(length(p))=0;

for i=3:(length(p)-3)
    b=round(n/2.1)+1;
    for j=1:n
        avp1(i)=p(i-b+j)+avp1(i);
    end
    avp1(i)=avp1(i)/n;
end
plot(t,avp1,t,p1)
```

Figure 45: Routine used for data smoothing via averaging

```
load('shot_45_combustion_driver_data.mat'); %Loads shot data in a
variable called "dataStruct"
load('shot_45_combustion_driver_sensitivity.mat'); %Loads all settings
t=dataStruct(:,1)*1e3; %Time variable, convert to ms
%The following load in pressure readings, converting from voltage to
%pressure in kPa
p1=dataStruct(:,3)*1e3/cell2mat(sens(3));
p2=dataStruct(:,4)*1e3/cell2mat(sens(4));
p3=dataStruct(:,5)*1e3/cell2mat(sens(5));
p4=dataStruct(:,6)*1e3/cell2mat(sens(6));
pend=dataStruct(:,2)*1e3/cell2mat(sens(2));
burster=dataStruct(:,9)*1e3;
plot(t,p1,t,p2,t,p3,t,p4,t,pend)
title(['Shot Number ',num2str(cell2mat(shotCell(2)))])
legend('P_1','P_2','P_3','P_4','P_{endwall}')
xlabel('Time (ms)')
ylabel('Pressure (kPa)')

%% FFt part
%range
b=1050;
e=1250;
%sampling freq
Fs=100000;

c=0;
for i=b:e
    c=1+c;
    fp(c)=p(i);
end

fp(:)=fp(:)-mean(fp);
plot(fp)
title('signal segment to apply FFT');
pause;

NFFT = 2^nextpow2(length(fp)); % Next power of 2 from length of y
Pfft = fft(fp,NFFT);
f = Fs/2*linspace(0,1,NFFT/2+1);

% Plot single-sided amplitude spectrum.
plot(f,2*abs(Pfft(1:NFFT/2+1)))
title('Single-Sided Amplitude Spectrum of y(t)')
xlabel('Frequency (Hz)')
ylabel('|Y(f)|')

pause;

%this is the limit for frequencies which are removed
d=mean(Pfft)+std(Pfft)*3;

%now find those frequencies
e=0;
for i=1:NFFT
    aa(i)=i;
    bb(i)=0;
    cc(i)=d;
```

Figure 46: Routine used for data smoothing via Fourier analysis (Page 1 of 3)

```
    if abs(Pfft(i))>d
        e=e+1;
        bf(e)=i;
        bb(i)=max(abs(Pfft));
    end
end

%plot cut off freq and what frequencies were picked
plot(aa,abs(Pfft(1:NFFT)),aa,bb,aa,cc)
title('Frequency cut off and those removed')
%plot(bf);
pause;

%now remove those frequencies, setting them to the mean value of the
fft
Mpfft=Pfft;
for i=1:length(bf)
    Mpfft(bf(i))=mean(Pfft);
end

%inverse fft and replot and compare
g=ifft(Mpfft);
for i=1:length(fp)
    h(i)=i;
    mfp(i)=g(i);
end

plot(c,fp,h,mfp)
title('Comparing raw to modified signal');
pause;

%convert position in Pfft to frequency, so they may be subtracted from
%full signal

%Take FFt of whole usable signal
b3=1020;
e3=2000;

c3=0;
for i=b3:e3
c3=1+c3;
    fp3(c3)=p(i);
end

fp3(:)=fp3(:)-mean(fp3);
plot(fp3);
title('Mean adjusted entire usable signal')
pause;

NFFT3 = 2^nextpow2(length(fp3)); % Next power of 2 from length of y
Pfft3 = fft(fp3,NFFT3);
f3 = Fs/2*linspace(0,1,NFFT3/2+1);

% Plot single-sided amplitude spectrum.
plot(f3,2*abs(Pfft3(1:NFFT3/2+1)),f,2*abs(Pfft(1:NFFT/2+1)))
title('Segment signal and Entire usable signal FFTs')
```

Figure 47: Routine used for data smoothing via Fourier analysis (Page 2 of 3)

```
xlabel('Frequency (Hz)')
ylabel('|Y(f)|')
pause;

%Remove previously found frequencies
MPfft3=Pfft3;
for i=1:NFFT3
    if bb(ceil(NFFT*i/NFFT3-i/NFFT3+1/i))>1
        MPfft3(i)=0;
    end
    if bb(ceil(NFFT*i/NFFT3-i/NFFT3+3/i))>1
        MPfft3(i)=0;
    end
end

plot(f3,2*abs(Pfft3(1:NFFT3/2+1)),f3,2*abs(MPfft3(1:NFFT3/2+1)),f,2*abs
(Pfft(1:NFFT/2+1)),f,bb(1:NFFT/2+1)) ;
title('Segment signal, Entire usable signal, and Modified Entire usable
signal FFTs')
pause;

g3=ifft(MPfft3);

for i=1:length(fp3)
    h3(i)=i;
    mfp3(i)=g3(i);
end

for i=1:length(fp3)
    c3(i)=i;
end
plot(c3,fp3,h3,mfp3)
title('Comparing raw to modified entire signal');
```

Figure 48: Routine used for data smoothing via Fourier analysis (Page 3 of 3)

C Checklist

Combustion Driven Shock Tube Checklist
Ae104c Experiment

Operators: _____

Date: _____ Time: _____

Shot number: _____

Run Conditions

Diaphgram material and thickness: _____

Driven section	**Driver section**	**Mixture**
Driven gas: _____	Driver gases: _____	Volume Fraction: _____
Desired P_1: _____	Expected P_4: _____	Desired PP's: _____
Actual P_1: _____	Actual P_4: _____	Actual PP's: _____

Comments:

_____

_____

_____

Positioning the diaphragm

- ◯ Cut diaphragm, record material and thickness
- ◯ **Use spanner wrench** to unscrew brass fitting joining the driver and driven sections
- ◯ Slide the driven section out carefully
- ◯ Remove the old diaphragm and place the new one against the diaphragm burster
- ◯ Gently slide the driven section back into place, making sure the diaphragm stays in place
- ◯ Screw brass fitting back into place and **tighten with spanner wrench**

Refilling Mixing Tank (Not necessary for every shot)

- ◯ Close A1 and A2
- ◯ Close RV1
- ◯ Close mixing tank valves DV1 and DV2
- ◯ Ensure all gas line needle valves are closed
- ◯ Open MIX1 and MIX2
- ◯ Open RV3
- ◯ Open RV2
- ◯ Plug in 6" tube vacuum pump
- ◯ Open RV4
- ◯ Wait for vacuum (< 1 Torr). Vacuum pressure: _____

Figure 49: Checklist used during experiments (Page 1 of 4)

Mixing Tank Filling Procedure

- ◯ **Earphones and eye protection on**
- ◯ Close RV2
- ◯ Open Helium bottle and regulator
- ◯ Open Helium fill line valve He, fill to desired partial pressure
- ◯ Record Helium PP
- ◯ Close Helium bottle, regulator, and He valve
- ◯ Close MIX2
- ◯ Close MIX1
- ◯ Open RV2 to vacuum panel lines
- ◯ Open Oxygen needle valve
- ◯ Wait for vacuum
- ◯ Close Oxygen needle valve
- ◯ Close RV2
- ◯ Open Oxygen bottle and regulator
- ◯ Open Oxygen needle valve on panel, fill panel lines above current pressure in tank
- ◯ Close Oxygen needle valve
- ◯ Open MIX1
- ◯ Slowly open Oxygen needle valve and fill to desired partial pressure
- ◯ Record Oxygen PP
- ◯ Close Oxygen bottle, regulator, and needle valve
- ◯ Close MIX1
- ◯ Open RV2 to vacuum panel lines
- ◯ Open Hydrogen needle valve
- ◯ Wait for vacuum
- ◯ Close Hydrogen needle valve
- ◯ Close RV2
- ◯ Open Hydrogen bottle and regulator
- ◯ Open Hydrogen needle valve on panel, fill panel lines above current pressure in tank
- ◯ Close Hydrogen needle valve
- ◯ Open MIX1
- ◯ Slowly open Hydrogen needle valve and fill to desired partial pressure
- ◯ Record Hydrogen PP
- ◯ Close Hydrogen bottle, regulator, and needle valve
- ◯ Close MIX1
- ◯ Turn on Mixing fan
- ◯ Open RV2 to vacuum panel lines
- ◯ Wait for vacuum
- ◯ Close RV2
- ◯ Unplug vacuum pump

Evacuation of shock tube

- ◯ **Earphones and eye protection on**
- ◯ Close A1 and A2
- ◯ Open FILL and VAC
- ◯ Turn on small vacuum pump
- ◯ Open SV
- ◯ Open DV1 and DV2
- ◯ Open GV2 and GV1 to lines

Figure 50: Checklist used during experiments (Page 2 of 4)

- ◯ Wait ∼10 minutes for vacuum. Vacuum pressure: _____
- ◯ Close SV
- ◯ Turn off small vacuum pump

Fill Driver and Fire

- ◯ Close VAC
- ◯ Slowly open A2 and A3 and fill to desired pressure, using needle valve to fill slowly. Record final pressure
- ◯ Close IV2
- ◯ Close A3
- ◯ Close A2
- ◯ Open GV1 to atmosphere
- ◯ Confirm Gauge 1 reads atmospheric pressure
- ◯ Open DV1 and DV2
- ◯ Open mixing tank valve MIX2
- ◯ Open DV1, slowly open DV2 and fill to desired pressure, iteravely checking pressure by closing DV1
- ◯ Record fill pressure
- ◯ Close IV1
- ◯ Open GV2 to atmosphere
- ◯ Confirm Gauge 2 reads atmospheric pressure
- ◯ Close DV1 and DV2
- ◯ Close MIX2
- ◯ Close FILL
- ◯ Ensure "Self-test" is off on DAS
- ◯ Turn ON burster box and spark plug box to begin charging capacitors
- ◯ Arm data acquisition system, ensure shot number is correct
- ◯ Wait until capacitors are fully charged
- ◯ Exit room, close door
- ◯ FIRE

Evacuation of shock tube

- ◯ Turn OFF burster and spark plug boxes
- ◯ Open A1
- ◯ Open IV1, wait for pressure to reach atmospheric
- ◯ Open VAC
- ◯ Open IV2
- ◯ Open Helium bottle and regulator
- ◯ Open Helium valve He
- ◯ Open DV1 and DV2 to flush out fill line and tube
- ◯ Close Helium bottle and regulator
- ◯ Close Helium valve He
- ◯ Close DV1 and DV2

If emptying mixing tank:

- ◯ Evacuate driver and fill lines
- ◯ Fill driver with mixture to 1 bar pressure
- ◯ Close MIX2
- ◯ Open Helium bottle, regulator, and fill valve He
- ◯ Fill to 2 bar pressure
- ◯ Close Helium bottle and regulator
- ◯ Close fill line valve He

Figure 51: Checklist used during experiments (Page 3 of 4)

◯ Open A1 to evacuate
◯ Repeat until mixing tank pressure is ¡ 1 bar, then leave MIX2 open when filling with helium

Opening and Cleaning shock tube

◯ Use spanner wrench to loosen brass fitting
◯ Open the shock tube and remove diaphragm
◯ Unplug ethernet cable from Gauge 1
◯ Unscrew Swagelok fitting from driven section endcap
◯ VERY gently unscrew and remove pressure transducer cable from endcap
◯ Unscrew and remove endcap from driven section
◯ Clean out debris with compressed air, blowing from front to back of the tube
◯ Clean out dirt and grime with "chimney sweep" if necessary
◯ Screw endcap back onto the driven section
◯ Gently reattach Swagelok fitting and pressure transducer cable
◯ Plug ethernet cable back into Gauge 1, confirm that readout displays atmospheric pressure

Figure 52: Checklist used during experiments (Page 4 of 4)

D Shot Data

			Experiment		Cantera Predictions		% Error	
Shot	p_1 (Pa)	p_4 (kPa)	u_s (m/s)	$p_2 - p_1$ (kPa)	u_s (m/s)	$p_2 - p_1$ (kPa)	u_s	$p_2 - p_1$
38	160	754	2714.00	7.17	2248.00	8.04	20.73	-10.86
40	420	763	2038.89	9.11	2020.00	16.79	0.94	-45.73
41	420	761	2075.74	12.38	2019.00	16.78	2.81	-26.23
42	160	755	2716.97	7.74	2249.00	8.04	20.81	-3.72
44	210	764	2471.40	7.73	2188.00	9.95	12.95	-22.29
45	260	757	2374.56	8.65	2135.00	11.70	11.22	-26.11
46	340	763	2139.55	8.13	2072.00	14.35	3.26	-43.36
47	420	757	1990.45	9.41	2018.00	16.76	-1.37	-43.83
48	540	757	1894.07	9.43	1955.00	20.14	-3.12	-53.18
49	660	757	1657.81	11.30	1903.00	23.27	-12.88	-51.43
50	860	755	1627.19	12.92	1834.00	28.03	-11.28	-53.92
51	1100	758	1780.92	12.54	1770.00	33.27	0.62	-62.32
52	420	756	2094.18	10.67	2018.00	16.75	3.78	-36.29
53	3000	758	1151.54	24.92	1500.00	63.78	-23.23	-60.93
54	43000	766	982.68	174.18	822.00	234.78	19.55	-25.81
55	420	756	1952.64	10.84	2018.00	16.75	-3.24	-35.26
56	19000	756	568.24	25.18	1011.00	168.00	-43.79	-85.01
1000	3000	756	870.49	12.48	2415.00	170.00	-63.95	-92.66

Table 5: Compiled data for experiments and Cantera predictions